

PHASEJUMPS: FAST COMPUTATION OF ZEROS FROM PLANAR GRID SAMPLES

ANTTI HAIMI, GÜNTHER KOLIANDER, AND JOSÉ LUIS ROMERO

ABSTRACT. We consider complex-valued functions on the complex plane and the task of computing their zeros from samples taken along a finite grid. We introduce PhaseJumps, an algorithm based on comparing changes in the complex phase and local oscillations among grid neighboring points. The algorithm is applicable to possibly non-analytic input functions, and also computes the direction of phase winding around zeros.

PhaseJumps provides a first effective means to compute the zeros of the short-time Fourier transform of an analog signal with respect to a general analyzing window, and makes certain recent signal processing insights more widely applicable, overcoming previous constraints to analytic transformations. We study the performance of (a variant of) PhaseJumps under a stochastic input model motivated by signal processing applications and show that the input instances that may cause the algorithm to fail are fragile, in the sense that they are regularized by additive noise (smoothed analysis). Precisely, given samples of a function on a grid with spacing δ , we show that our algorithm computes zeros with accuracy $\sqrt{\delta}$ in the Wasserstein metric with failure probability $O(\log^2(\frac{1}{\delta})\delta)$, while numerical experiments suggests even better performance.

1. INTRODUCTION

1.1. Computation of zero sets from grid values. Let $F: \mathbb{C} \rightarrow \mathbb{C}$ be a continuous function and consider the problem of computing an approximation of its zero set within the box

$$(1.1) \quad \Omega_L = \{x + iy : |x|, |y| \leq L\}.$$

We assume that we have access to the values of F only on those points from the grid

$$(1.2) \quad \Lambda = \{\delta k + i\delta j : k, j \in \mathbb{Z}\}$$

that lie inside (or very near) the *computation domain* Ω_L . We think of the inverse of the grid spacing δ as the *resolution of the data*.

When F is analytic, the Minimal Grid Neighbors (MGN) algorithm provides a fast and highly effective way to carry out the desired computation. The method consists in collecting all grid points $\lambda \in \Lambda \cap \Omega_L$ for which the weighted magnitude $e^{-|\lambda|^2/2}|F(\lambda)|$ is minimal among all the immediate grid neighbors of λ :

$$(1.3) \quad e^{-|\lambda|^2/2}|F(\lambda)| \leq e^{-|\lambda'|^2/2}|F(\lambda')|, \quad \lambda' \in \Lambda, \quad |\lambda' - \lambda|_\infty = \delta.$$

2020 *Mathematics Subject Classification.* 60G15, 60G55, 94A12, 42A61.

Key words and phrases. Short-time Fourier transform, spectrogram, zeros set, charge, critical point, random function, Wasserstein metric, Gaussian Weyl-Heisenberg Function.

This research was funded in whole or in part by the Austrian Science Fund (FWF): 10.55776/Y1199. For open access purposes, the authors have applied a CC BY public copyright license to any author-accepted manuscript version arising from this submission.

(This requires access to F not only on the grid points $\Lambda \cap \Omega_L$ but on the slightly larger set of all their immediate grid neighbors.) The MGN algorithm was implicitly introduced in [16] and has since become an important tool in signal processing, where the *short-time Fourier transform* of a signal is given on a grid, and its zeros are used as landmarks that help distinguish signal components from noise (see Section 1.3). While no algorithm can work for all possible input function (as the values of F on a finite grid do not determine F elsewhere), the remarkable effectiveness of (a slight variant of) MGN has been theoretically validated under a stochastic input model aimed at describing its performance in practice [14, 30].

Unfortunately, the MGN algorithm does not work well with non-analytic input functions F , because the success of the minimality test (1.3) in finding zeros depends crucially on the superharmonicity of the weighted function $e^{-|z|^2/2}|F(z)|$ (see [26, Section 8.2.2] and [14, Lemma 3.1]). This restriction limits the applicability of filtering methods based on short-time Fourier transform zeros, as many time-frequency representations used in practice are non-analytic.

In this article we introduce and analyze a new algorithm, called PhaseJumps, that provides fast computation of zero sets of possibly non-analytic functions from their values on a finite grid. As we discuss in Section 1.3, this provides a first means to compute the zeros of general time-frequency representations.

1.2. The PhaseJumps algorithm. Consider again the problem of computing the zero set $\{F = 0\} \cap \Omega_L$ of a possibly non-analytic function F . The PhaseJumps algorithm identifies certain points on the finite grid

$$\Lambda_L := \Lambda \cap \Omega_L = \{\delta k + i\delta j : k, j \in \mathbb{Z}, |\delta k|, |\delta j| \leq L\}$$

as numerical approximations of zeros, by detecting changes of the complex argument (phase) around those points. The key parameter of the algorithm is a choice of *phase-stabilizing factors*

$$\nu(z, w) \in \mathbb{C} \setminus \{0\}, \quad z, w \in \mathbb{C},$$

which are only required to depend differentiably on (z, w) (in the real sense). Once the factors are fixed, the corresponding *phase-stabilized shifts* are

$$(1.4) \quad F_w(z) = \nu(z, w)F(z + w), \quad z, w \in \mathbb{C}.$$

The default choice for the stabilizing factors is $\nu(z, w) = 1$, in which case (1.4) are the standard Euclidean translations. Later, we will choose $\nu(z, w) = e^{-i\text{Im}(z\bar{w})}$ and show that these factors are effective in applications to time-frequency analysis; see Figure 1 (left). We think of $F \mapsto F_w$ as a centering operation; independently of the particular choice of the (non-vanishing) phase-stabilizing factors, the phase winding of $F_w(z)$ near $z = 0$ coincides with that of $F(z)$ near $z = w$.

The PhaseJumps algorithm determines which boxes of half side-length 2δ centered at $\lambda \in \Lambda_L$ contain zeros of F by computing an approximation of the argument change along the boundary of the box. Specifically, we enumerate all points μ_j of the grid Λ with $|\mu_j|_\infty = 2\delta$ anti-clockwise and keep λ if

$$(1.5) \quad \sum_{j=1}^N \arg [F_\lambda(\mu_j) \overline{F_\lambda(\mu_{j-1})}] \neq 0.$$

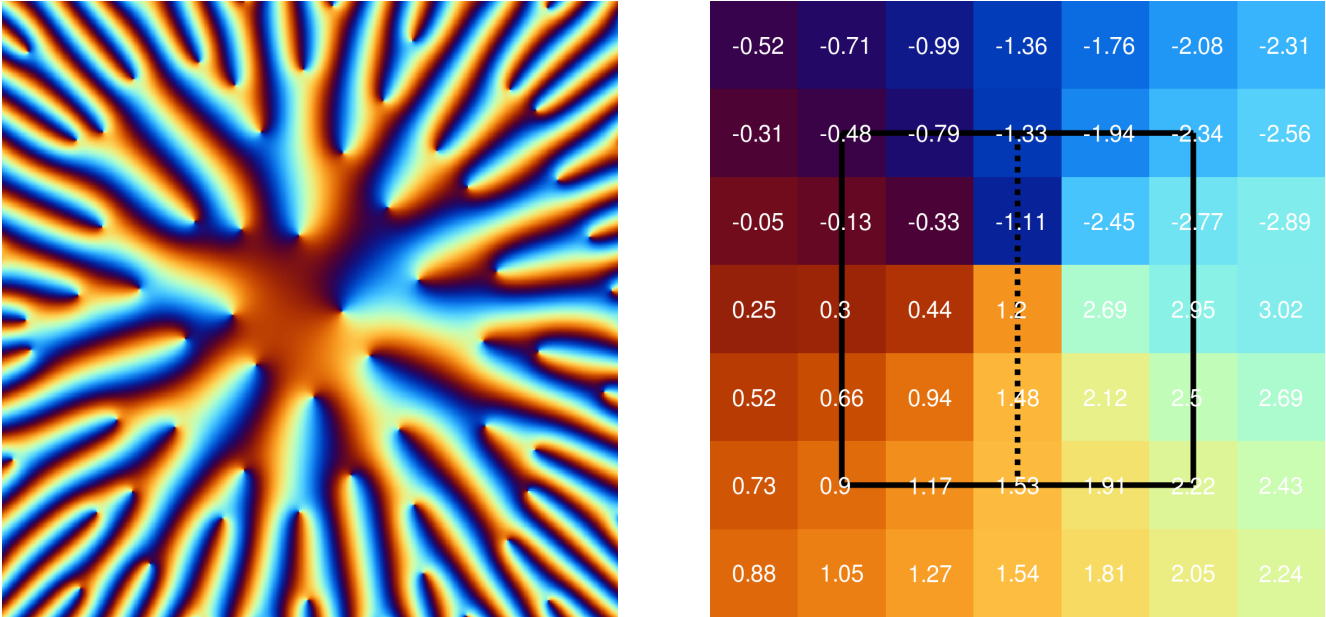


FIGURE 1. Phase values of a complex-valued function. *Left*: In applications to time-frequency analysis (see Section 1.3), phases fluctuate moderately near the origin but strongly away from it. The twisted shifts (1.8) re-center the function while moderating phase fluctuations, as in the center of the image. *Right*: A zoom onto the pixel values close to a potential zero near the center. By calculating the argument change along the black square, we can deduce that a zero is likely within the box. This is justified because phase fluctuates moderately along the black box. On the other hand, along the dotted vertical segment, there is a large argument jump.

Here $\arg: \mathbb{C} \setminus \{0\} \rightarrow (-\pi, \pi]$ is the principal branch of the argument, which we further define for convenience as $\arg(0) := 0$. Of course, this approximate computation of the argument change may be incorrect if the argument of F changes very significantly between grid neighbors. We take this possibility into account by eliminating λ as a candidate zero if the maximal argument fluctuation of F along neighboring points in the boundary of the test box is larger than 90% of the total possible argument change. More precisely, we only keep λ if, in addition to (1.5), the following holds:

$$(1.6) \quad \max_{j=1, \dots, N} \left| \arg \left[F_\lambda(\mu_j) \overline{F_\lambda(\mu_{j-1})} \right] \right| < 0.9 \cdot \pi.$$

The test box is taken to have half side-length 2δ (instead of $\delta/2$) because we expect the test (1.5) to be more reliable for detecting zeros well within the box. For zeros near the boundary of the test box, the phase fluctuations may be large and (1.6) may fail. We expect such a zero to be however caught by another test box centered close to it; see Figure 1.

The disadvantage of using slightly larger test boxes is redundancy: test boxes centered at neighboring points overlap and may cause multiple detections of the same zero. We compensate for this by *sieving* the set of selected points to enforce a minimal separation of 6δ between different points. The resulting set is the output of PhaseJumps, and our approximation of the zero set $\{F = 0\} \cap \Omega_L$.

Along the way, we have also computed the argument change (1.5), which, as we shall see, informs us about the *charge of F* at the detected zero z :

$$\kappa_z = \operatorname{sgn} \det DF(z) \in \{-1, 0, 1\},$$

where $DF(z)$ is the differential matrix of $F: \mathbb{R}^2 \rightarrow \mathbb{R}^2$. The charge of F at a zero z describes how F locally transforms orientation, and is a meaningful feature for non-analytic functions (while the conformality of analytic functions implies that their charges are always non-negative.)

The algorithm is formally specified as follows.

Algorithm PhaseJumps:

Compute the (charged) zero set of F inside the target domain $\Omega_L = [-L, L]^2$.

Input: A domain length $L \geq 1$, a grid spacing parameter $\delta > 0$, and samples of a function $F: \mathbb{C} \rightarrow \mathbb{C}$ on the grid points $\Lambda_{L+2\delta} = \Lambda \cap [-(L+2\delta), L+2\delta]^2$.

Parameter: A collection of phase-stabilizing factors $\{\nu(z, w) : z, w \in \mathbb{C}\} \subset \mathbb{C} \setminus \{0\}$.

Step 1. Set $Z_1 := \Lambda \cap \Omega_L$. For each $\lambda \in Z_1$, consider all $\mu \in \Lambda$ such that $|\mu|_\infty = 2\delta$, and order them as μ_1, \dots, μ_N so that $\arg(\mu_1) \leq \dots \leq \arg(\mu_N)$. Set $\mu_0 := \mu_N$.

Define

$$\theta_\lambda := \frac{1}{2\pi} \sum_{j=1}^N \arg [F_\lambda(\mu_j) \overline{F_\lambda(\mu_{j-1})}]$$

and

$$\chi_\lambda := \max_{j=1, \dots, N} \left[\frac{1}{\pi} \left| \arg [F_\lambda(\mu_j) \overline{F_\lambda(\mu_{j-1})}] \right| \right].$$

Let $Z_2 := \{\lambda \in Z_1 : \theta_\lambda \neq 0 \text{ and } \chi_\lambda < 0.9\}$.

Step 2. Use an off-the-shelf clustering algorithm to select a subset $Z \subset Z_2$ such that elements with the same θ_λ are 6δ separated:

$$(1.7) \quad \inf \{|\lambda - \lambda'| : \lambda, \lambda' \in Z, \theta_\lambda = \theta_{\lambda'}, \lambda \neq \lambda'\} \geq 6\delta$$

and is maximal with respect to that property, i.e., no proper superset satisfies (1.7).

Output: The set Z and the numbers $\{\theta_\lambda : \lambda \in Z\}$.

(Note that the tests in Step 1 and 2 only involve grid points $\lambda + \mu_j \in \Lambda_{L+2\delta}$.)

We note that PhaseJumps is very fast and can be used on large data sets.

1.3. Twisted PhaseJumps and Gabor analysis. In the remainder of the article, we consider $\nu(z, w) = e^{-i \operatorname{Im}(z\bar{w})}$ as phase-stabilizing factors in (1.4), which yields the *twisted shifts*

$$(1.8) \quad F_w(z) = F(z + w)e^{-i \operatorname{Im}(z\bar{w})}, \quad z, w \in \mathbb{C}.$$

We refer to the corresponding algorithm as Twisted PhaseJumps. This choice of phase stabilization is tailored to applications in non-stationary signal processing, as we now briefly explain.

The goal of *Gabor analysis* is to analyze a so-called *signal* $f: \mathbb{R} \rightarrow \mathbb{C}$ by means of certain discrete time-frequency measurements, known as *Gabor coefficients*. These encode the correlations

of f with the time and frequency shifts of a reference Schwartz class *window function* $g: \mathbb{R} \rightarrow \mathbb{C}$:

$$(1.9) \quad c_{k,j} = \int_{\mathbb{R}} f(t) \overline{g(t - \delta k)} e^{-2\pi i \delta j t} dt, \quad k, j \in \mathbb{Z},$$

where the resolution parameter $\delta > 0$ is essentially determined by the quality of the analog-to-digital conversion device.¹

In essence, Gabor analysis is about *sampling*, because the coefficients (1.9) are the values of the *short-time Fourier transform of f* :

$$(1.10) \quad V_g f(x, \xi) = \int_{\mathbb{R}} f(t) \overline{g(t - x)} e^{-2\pi i \xi t} dt, \quad (x, \xi) \in \mathbb{R}^2$$

on the grid (1.2): $c_{k,j} = V_g f(\delta k, \delta j)$. While the full collection of time-frequency correlations (1.10) completely determines the signal f , Gabor analysis aims to extract information about f (or, equivalently, about $V_g f$) from the coefficients (1.9), or, more realistically, from a finite subcollection thereof.

We are motivated by the problem of learning the *zero set* of $V_g f$ from finite data of the form (1.9). The zero set in question has been recently discovered to provide a rich set of landmarks [19] that help identify a non-stationary signal impacted by additive noise [16, 17, 6, 20]. Specifically, empirical statistics for zeros – computed with a particular signal f – are compared to ensembles averages under a certain noise model, for which precise statistics are known [26, 24, 6, 7, 22, 14, 15]. *This paradigm necessitates, however, an efficient method to compute the desired zero set from finite data*, something that so far has only been available for the Gaussian window function $g(t) = e^{-\pi t^2}$. Indeed, in this special case, the change of variables

$$(1.11) \quad F(z) = e^{-ix\xi} \cdot V_g f(x/\sqrt{\pi}, -\xi/\sqrt{\pi}), \quad z = x + i\xi,$$

yields a weighted analytic function, and the Minimal Grid Neighbors algorithm [16] computes its zeros very efficiently (see Section 1.1).² In contrast, for non-Gaussian window functions g , the short-time Fourier transform cannot be identified with a weighted analytic function [3] and the MGN algorithm is not effective (see Section 1.1). This is a shortcoming in many important applications where it is helpful to use and to average over several (non-Gaussian) window functions [18, Section 10.2].

1.4. Contribution. Our contribution is two-fold. First, PhaseJumps provides, for the first time, an effective method to compute the zeros of the short-time Fourier transform with an arbitrary window. As an illustration, Figure 2 shows the computation of the zeros and charges of the STFT of the signal $f(t) = e^{-t^2/2}$ embedded into white noise, with respect to the window $g(t) = te^{-t^2/2}$; see also Section 5 for more comprehensive numerical experiments. Second, we provide the first theoretical guarantees for the computation of zeros of short-time Fourier transforms (with general windows) from grid-values. While in practice Twisted PhaseJumps effectively approximates the desired zero set $\{F = 0\} \cap \Omega_L$ of the function (1.11) up to a resolution comparable to that of the acquisition grid (1.2), we shall only prove that computations are accurate up to the coarser scale

¹This is of course a simplified digital acquisition model. In practice, signals are often quantized in time and then processed, which introduces other errors that we do not model with (1.9).

²The description of the algorithm in Section 1.1 pertains to the analytic function $\tilde{F}(z) = e^{|z|^2/2} F(z)$ in lieu of $F(z)$ and thus involves the local minima of $|F(\lambda)|$.

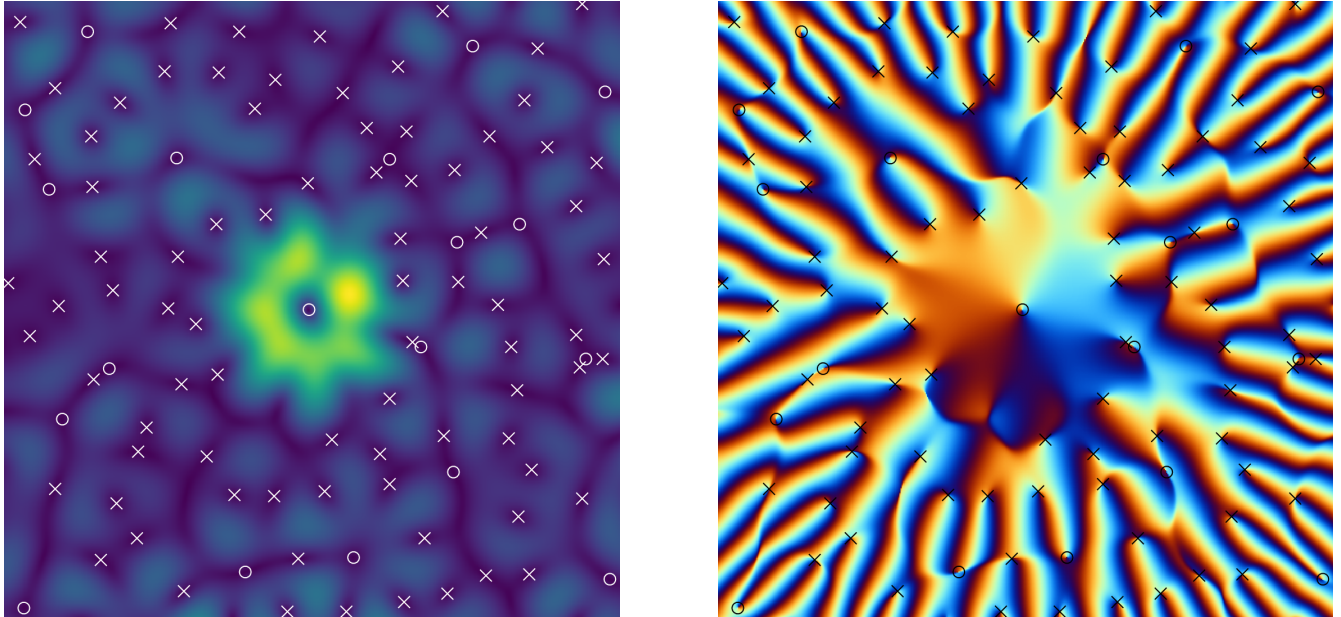


FIGURE 2. The STFT of a Gaussian signal in additive complex white noise using the first Hermite function as window (*Left: Modulus, Right: Phase*). Zeros with positive charge are marked by \times and zeros with negative charge by \circ .

$\sqrt{\delta}$. To facilitate the presentation, we shall introduce a modified version of Twisted PhaseJumps, which we call Twisted PhaseJumps-coarse, that explicitly deals with two scales, corresponding to data and computation resolution levels.

Our work also has novel applications to spectrograms computed with Gaussian windows. While such functions are or can be identified with analytic functions – and therefore their zeros can be effectively computed with MGN [18] – other landmarks such as *spectrogram local maxima and saddle points* are related to zeros and charges of the short-time Fourier transform with Hermite windows; see, e.g., [22, Section 6.8], [15, Section 9.2]. Thus our work provides for the first time a reliable means to compute such features, which are important in relation to spectrogram reassignment [18, Chapters 12 and 14]; see Figure 3.

In the same vein, by applying PhaseJumps to simulated inputs, we provide a first efficient means to simulate *critical points of random entire functions* – which are zeros of certain non-analytic functions, and provide heuristic models in string theory [12]. Similarly, PhaseJumps enables the simulation of zeros of higher order random poly-entire functions [21, 22], a task that has so far been very challenging.

2. SMOOTHED ANALYSIS AT LOWER COMPUTATIONAL RESOLUTION

2.1. The PhaseJumps-coarse algorithm. Consider again the problem of computing the zero set $\{F = 0\} \cap \Omega_L$ of a possibly non-analytic function F , and let us introduce the following *coarse sub-grid* of Λ :

$$(2.1) \quad \Delta = \{\delta^* k + i\delta^* j : k, j \in \mathbb{Z}\}, \text{ with } \delta^* := 2 \lceil \delta^{-1/2}/4 \rceil \delta,$$

which has spacing $\delta^* \approx \sqrt{\delta}$. The Twisted PhaseJumps-coarse algorithm chooses some points of the finite grid

$$\Delta_L := \Delta \cap \Omega_L = \{\delta^*k + i\delta^*j : k, j \in \mathbb{Z}, |\delta^*k|, |\delta^*j| \leq L\}$$

as numerical approximations of zeros, by applying three consecutive selection tests, formulated in terms of the twisted shifts (1.8).

Step 1. We compare oscillations relative to the *fine scale* δ and the *coarse scale*

$$\delta^{**} := \lceil \delta^{-1/2} \rceil \delta.$$

A point $\lambda \in \Delta_L$ is selected if

$$|F_\lambda(\mu)| \geq 2|F_\lambda(\mu) - F_\lambda(\mu')|,$$

whenever $\mu, \mu' \in \Lambda$ are such that

$$|\mu|_\infty = |\mu'|_\infty = \delta^{**}, \text{ and } |\mu' - \mu|_\infty = \delta.$$

(Here, F_λ is the twisted shift, cf. (1.8).) This test is a variant of the small phase-oscillation condition (1.6) that is better suited to the two-scale setting. Intuitively, the test is satisfied whenever F vanishes near λ , because then the points μ at the boundary of the box of half side-length $\delta^{**} \approx \sqrt{\delta}$ satisfy $|F_\lambda(\mu)| \approx |F'_\lambda(\mu)|\sqrt{\delta}$, while the oscillations at the fine scale are $|F_\lambda(\mu) - F_\lambda(\mu')| \approx |F'_\lambda(\mu)|\delta$, and the margin between the coarse and fine scale is wide enough to allow us to neglect second order errors.

Step 2. In the same spirit as PhaseJumps, we then try to decide which boxes of half side-length δ^{**} centered at the previously selected points λ contain zeros of F by computing an approximation of the argument change along the boundary of the box. We enumerate all points μ_j of the fine grid Λ with $|\mu_j|_\infty = \delta^{**}$ anti-clockwise and keep λ only if

$$\sum_{j=1}^N \arg [F_\lambda(\mu_j) \overline{F_\lambda(\mu_{j-1})}] \neq 0.$$

Step 3. Finally, we sieve the obtained set to enforce a minimal separation of $5\delta^{**}$ between different points.

The algorithm is formally specified as follows.

Algorithm Twisted PhaseJumps-coarse:

Compute the (charged) zero set of F inside the target domain $\Omega_L = [-L, L]^2$.

Input: A domain length $L \geq 1$, a grid spacing parameter $\delta > 0$ and samples of a function $F: \mathbb{C} \rightarrow \mathbb{C}$ on the grid points $\Lambda_{L+\delta^{**}} = \Lambda \cap [-(L + \delta^{**}), L + \delta^{**}]^2$, where $\delta^{**} := \lceil \delta^{-1/2} \rceil \delta$.

Step 1: A point $\lambda \in \Delta_L$ is *selected* if

$$(2.2) \quad |F_\lambda(\mu)| \geq 2|F_\lambda(\mu) - F_\lambda(\mu')|,$$

whenever $\mu, \mu' \in \Lambda$ are such that

$$(2.3) \quad |\mu|_\infty = |\mu'|_\infty = \delta^{**}, \text{ and } |\mu' - \mu|_\infty = \delta.$$

Let Z_1 be the set of all selected points.

Step 2. For each $\lambda \in Z_1$, consider all $\mu \in \Lambda$ such that $|\mu|_\infty = \delta^{**}$, and order them as μ_1, \dots, μ_N so that $\arg(\mu_1) \leq \dots \leq \arg(\mu_N)$. Set $\mu_0 := \mu_N$.

If $F_\lambda(\mu_j) = 0$ for some $j = 1, \dots, N$, set $\theta_\lambda := 0$. Otherwise, define

$$(2.4) \quad \theta_\lambda := \frac{1}{2\pi} \sum_{j=1}^N \arg [F_\lambda(\mu_j) \overline{F_\lambda(\mu_{j-1})}].$$

Let $Z_2 := \{\lambda \in Z_1 : \theta_\lambda \neq 0\}$.

Step 3. Use an off-the-shelf clustering algorithm to select a subset $Z \subset Z_2$ that is $5\delta^{**}$ separated:

$$(2.5) \quad \inf \{|\lambda - \lambda'|_\infty : \lambda, \lambda' \in Z, \lambda \neq \lambda'\} \geq 5\delta^{**}$$

and is maximal with respect to that property, i.e., no proper superset satisfies (2.5).

Output: The set Z and the numbers $\{\theta_\lambda : \lambda \in Z\}$.

(Note that the tests in Steps 2 and 3 only involve grid points $\lambda + \mu, \lambda + \mu', \lambda + \mu_j \in \Lambda_{L+\delta^{**}}$.)

We stress that Twisted PhaseJumps-coarse is not introduced as a competitive algorithm, but only as a means to approximately analyze the performance of Twisted PhaseJumps, which is the preferred option in practice.

2.2. Smoothed analysis. We now analyze Twisted PhaseJumps-coarse under a stochastic input model that is designed to describe its performance in practice. As input, we consider a random function $F: \mathbb{C} \rightarrow \mathbb{C}$ on the complex plane of the form:

$$(2.6) \quad F = F^1 + \sigma F^0,$$

where $F^1: \mathbb{C} \rightarrow \mathbb{C}$ is deterministic, F^0 is a zero mean random function with distribution to be specified, and $\sigma > 0$ is the *noise level*.

We will derive probabilistic guarantees that are uniform over an adequate class of deterministic functions F^1 and depend explicitly on the noise level σ and other relevant parameters such as the grid spacing δ . This form of analysis, known as *smoothed analysis* [30], lies between worst case and average case analysis, and to a great extent inherits the benefits of both. While average case analysis can show that an algorithm succeeds for generic or zero mean random inputs, these rarely model inputs found in practice. In contrast, smoothed analysis measures the performance of the algorithm under slight perturbations of possibly worst case inputs, and can show that *theoretically bad inputs are fragile* in the sense that a moderate amount fluctuation, as often encountered in practice, can restore good performance. In applications to the short-time Fourier transform (see Section 1.3) smoothed analysis is closely related to the so-called *noise assisted methods*, see, e.g. [34, 10, 9, 32].

2.3. Input model. We consider the random function (2.6) and specify F^0 and F^1 . The assumptions we make are motivated by the application introduced in Section 1.3, so that, under the change of variables (1.11), F corresponds to the short-time Fourier transform $V_g f$ of a random distribution³ on \mathbb{R} :

$$(2.7) \quad f = f^1 + \sigma f^0,$$

³Here, we assume that the window function g is Schwartz and we interpret (1.10) distributionally.

where f^0 is standard (complex, Gaussian) white noise on \mathbb{R} [25], $\sigma > 0$ is the noise level, and f^1 is an arbitrary distribution with bounded short-time Fourier transform⁴ – a condition satisfied by any L^2 function, and also by all distributions commonly used in signal processing (Dirac deltas, periodizations and Fourier transforms thereof, etc.) [8].

We now spell out concrete assumptions. To quantify the smoothness and decay of F^1 we use the *twisted derivatives*:

$$(2.8) \quad \mathcal{D}_1 F(z) = \partial F(z) - \frac{\bar{z}}{2} F(z), \quad \mathcal{D}_2 F(z) = \bar{\partial} F(z) + \frac{z}{2} F(z),$$

where $\partial F(x + iy) = \frac{1}{2}(\partial_x F(x + iy) - i\partial_y F(x + iy))$ and $\bar{\partial} F(x + iy) = \frac{1}{2}(\partial_x F(x + iy) + i\partial_y F(x + iy))$ are the usual complex derivatives. The merit of the twisted derivatives is that they commute with the twisted shifts (1.8).

We assume that F^1 is twice continuously differentiable (in the real sense) and, moreover,

$$(2.9) \quad A := \max \{ \|F^1\|_\infty, \|\mathcal{D}_i F^1\|_\infty, \|\mathcal{D}_i \mathcal{D}_j F^1\|_\infty : i, j = 1, 2 \} < \infty.$$

The random function F^0 is assumed to be a circularly symmetric complex Gaussian random field on \mathbb{C} with covariance kernel

$$(2.10) \quad \mathbb{E} \left[F^0(z) \cdot \overline{F^0(w)} \right] = H(z - w) e^{i \operatorname{Im}(z\bar{w})}, \quad z, w \in \mathbb{C},$$

where $H : \mathbb{C} \rightarrow \mathbb{C}$ is a function called *twisted kernel*. Concretely this means that for every $z_1, \dots, z_n \in \mathbb{C}$, the complex random vector $(F(z_1), \dots, F(z_n))$ is normally distributed, circularly symmetric, with mean zero and covariance matrix $(H(z_k - z_j) e^{i \operatorname{Im}(z_k \bar{z}_j)})_{k,j}$.

The particular structure of the covariance kernel is a form of stationarity introduced in [22] under the name of *twisted stationarity*. It means that the stochastics of F^0 are invariant under twisted shifts:

$$\mathbb{E} \left[F^0(z) \cdot \overline{F^0(w)} \right] = \mathbb{E} \left[F_w^0(z) \cdot \overline{F_w^0(w)} \right], \quad w \in \mathbb{C}.$$

Of the twisted covariance kernel, we assume that

$$(2.11) \quad H \in C^6 \text{ in the real sense}$$

and impose the normalization

$$(2.12) \quad H(0) = 1,$$

which means that $\operatorname{Var}[F^0(z)] = 1$. Consequently σ^2 is the noise variance in (2.6). We also assume that

$$(2.13) \quad |H(z)| < 1, \quad z \in \mathbb{C} \setminus \{0\},$$

which means that $F(z), F(w)$ are not deterministically correlated if $z \neq w$ — because the determinant of their joint covariance matrix is $1 - |H(z - w)|^2$. We also assume that F is almost surely C^2 . Since H is smooth, this is automatically the case, as long as a certain mild technical condition known as *separability* is satisfied; see [1, Section 1.1] [4, Chapter 1].

As we discuss in Section 3.4 and Lemma 3.3, for f as in (2.7) and

$$F(x + iy) := e^{-ixy} \cdot V_g f(x/\sqrt{\pi}, -y/\sqrt{\pi}),$$

⁴In the jargon of time-frequency analysis, we say that f^1 belongs to the *modulation space* $M^\infty(\mathbb{R})$ [8].

all assumptions are satisfied with $H(x+iy) = e^{-ixy} \cdot V_g g(x/\sqrt{\pi}, -y/\sqrt{\pi})$. In this case, the constant (2.9) is $A \asymp \|V_g f\|_\infty$, so that A/σ can be interpreted as a signal-to-noise ratio. There are also other interesting instances of the input model, such as *random poly-entire functions* [21, 22], which are important in mathematical physics [2, 33].

Remark 2.1. As we show in Lemma 3.9, under this input model, the zero set of F is almost surely a discrete set (that is, each zero is isolated).

2.4. Performance guarantees. Our main theoretical result gives guarantees for the computation of the zero set of a function F restricted to the square (1.1) from grid samples, providing an estimate for the Wasserstein distance between the atomic measures supported on the true zero set $\{F = 0\} \cap \Omega_L$ and on the computed set Z (up to a small boundary effect). For simplicity we assume that the corners of the computation domain lie on the coarse grid (2.1).

Theorem 2.2. *Fix a domain width $L \geq 1$, a noise level $\sigma > 0$ and a grid resolution parameter $\delta > 0$ such that $L/\delta^* \in \mathbb{N}$. Let a realization of a random function F as in (2.6), with (2.9), (2.10), (2.11), (2.12), (2.13), be observed on the grid $\Lambda_{L+\delta^{**}}$ and let Z be the output of the Twisted PhaseJumps-coarse algorithm. Then there exist constants $C, c > 0$ such that with probability at least*

$$(2.14) \quad 1 - C \cdot L^2 \cdot \left(\log \frac{1}{\delta}\right)^2 \cdot \exp\left(cA^2/\sigma^2\right) \cdot \delta$$

there is an injective map $\Phi: \{F = 0\} \cap \Omega_L \rightarrow Z$ with the following properties:

- (Each zero is mapped into a near-by numerical zero)

$$(2.15) \quad |\Phi(\zeta) - \zeta|_\infty \leq 2\sqrt{\delta}, \quad \zeta \in \{F = 0\} \cap \Omega_L.$$

- (Each numerical zero that is away from the boundary arises in this way)
For each $\lambda \in Z \cap \Omega_{L-\delta^{**}}$ there exists $\zeta \in \{F = 0\} \cap \Omega_L$ such that $\lambda = \Phi(\zeta)$.
- (Winding numbers are accurately computed)

$$(2.16) \quad \kappa_\zeta = \theta_{\Phi(\zeta)}, \quad \zeta \in \{F = 0\} \cap \Omega_L.$$

(Here, the constants $C, c > 0$ depend on the twisted kernel H , cf. (2.10).)

2.5. Technical overview and comparison with other work. To our knowledge, the Minimal Grid Neighbors (MGN) algorithm described in Section 1.1 is the most effective method to compute zeros of *weighted analytic functions* from grid values. In our experience, other methods such as thresholding (using small values as proxies for zeros) or extrapolation (using the grid samples to approximately evaluate the function at an arbitrary point, so as to, say, apply an iterative root finder) lack the effectiveness or simplicity of MGN (see e.g., [14, Sections 1.2 and 5]) and are not preferred in practice. Notwithstanding, certain proposed homotopy algorithms [11] use MGN as an initialization step. While we are not aware of performance guarantees for MGN, a slight variation of MGN — called Adapted Minimal Grid Neighbors (AMN) — was introduced and analyzed in [14]. We developed PhaseJumps to address the problem of computing zeros of possibly *non-analytic functions* as cost effectively as with MGN/AMN.

Let us now compare the performance guarantees that we prove for Twisted PhaseJumps-coarse to those available for AMN. The following compares Theorem 2.2 to [14, Theorem 2.2], which

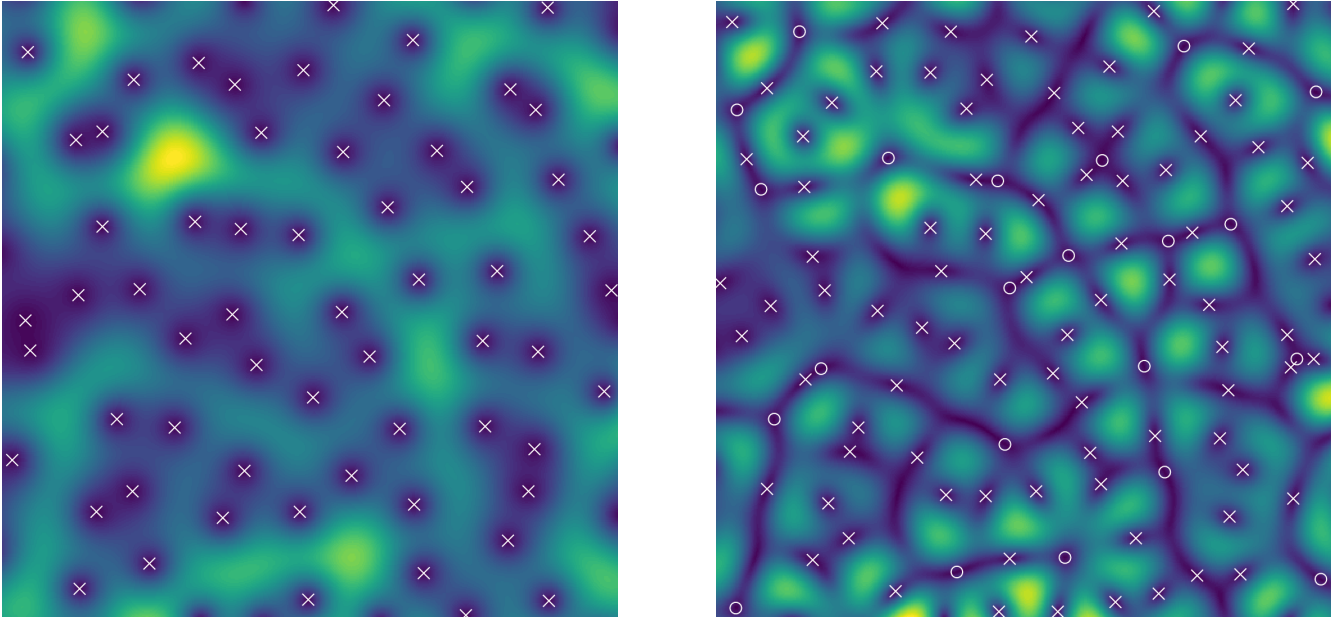


FIGURE 3. The squared absolute value of the STFT of (the same realization of) complex white noise using a Gaussian (left) or first Hermite function (right) as window, together with their zeros of positive (crosses) and negative (circles) charge. On the left-hand side, the magnitude increases locally at the same rate in all directions; on the right-hand side, zeros lie along “low-magnitude curves” (approximate nodal curves), which explains the difficulty in their computation. The positively (resp. negatively) charged zeros on the right-hand side correspond exactly to the saddle-points (resp. local maxima) of the function on the left-hand side.

provides an estimate of the Wasserstein distance between the atomic measures supported on the true zero set of an analytic function and the set computed by AMN.

- The input model considered in [14] is a particular instance of the one introduced in Section 2.3: there, functions are assumed to be analytic, while here functions may be non-analytic — see also Lemma 3.3.
- The failure probability in Theorem 2.2 is $O(\log^2(1/\delta) \cdot \delta)$, while the corresponding statement in [14, Theorem 2.2] fails with probability $O(\log^2(1/\delta) \cdot \delta^4)$.
- The maximal distortion in Theorem 2.2 is $O(\delta^{1/2})$, while that in [14, Theorem 2.2] is $O(\delta)$.

We believe that the weaker performance proved for Twisted PhaseJumps-coarse in comparison to AMN is not an artifact of our argument, but rather that it is commensurate with the fundamentally more challenging task of finding zeros of non-analytic inputs. Indeed, the zero set of a non-zero analytic function F is discrete, and, moreover, becomes well-separated after a moderate amount of noise is added to F [14]. In contrast, zeros of non-analytic functions can lie along curves, which persists as *almost nodal curves* after adding randomness; see Fig. 3 for an illustration in the context of the short-time Fourier transform. Thus, in comparison to the analytic case, much more randomness is required to regularize the zero set and turn it into a well-spread point pattern

[5, 23]. In fact, as we show in Section 3, analytic inputs form a “thin” set within our input model, and substantial effort is put into treating it separately, as a degenerate case (cf. Propositions 3.8 and 3.12).

In the formulation of Theorem 2.2 and the organization of its proof we tried to parallel those of [14], so as to better highlight the key differences between the analytic and non-analytic scenarios. Notably, as non-analytic functions depend non-trivially on the variables z and \bar{z} , linearization arguments are much more subtle because of different growth rates in different directions; see Fig. 3. Another central technical challenge in the present setting is that zeros are detected by means of topological index formulae, rather than by subharmonicity considerations, which requires new arguments. While the proofs in [14] rely on the theory of Gaussian Entire Functions [28, 26], in this article we use and further develop the parallel theory of Gaussian Weyl-Heisenberg Functions [22, 15].

2.6. Organization. The remainder of the article is organized as follows. Section 3 analyzes the stochastic input model and the geometry of the corresponding zero sets and winding numbers. Section 4 provides a proof of Theorem 2.2. In Section 5, we provide several numerical experiments that illustrate the effectiveness of PhaseJumps in time-frequency analysis and the need for twisted shifts, together with an empirical comparison with Twisted PhaseJumps-coarse, which shows that PhaseJumps should be preferred in practice.

3. ANALYSIS OF THE INPUT MODEL

3.1. Preliminaries and notation. Closed cubes are denoted $Q_r(w) := \{z \in \mathbb{C} : |z - w|_\infty \leq r\}$, while open disks are denoted $D_r = \{z \in \mathbb{C} : |z| < r\}$. The *twisted shifts* are defined by (1.8). We let $\arg: \mathbb{C} \setminus \{0\} \rightarrow (-\pi, \pi]$ denote the principal branch of the argument, and we further set $\arg(0) := 0$ for convenience.

The complex derivatives (Wirtinger operators) of a function $F: \mathbb{C} \rightarrow \mathbb{C}$ are:

$$\begin{aligned}\partial F(x + iy) &= \frac{1}{2}(\partial_x F(x + iy) - i\partial_y F(x + iy)), \\ \bar{\partial} F(x + iy) &= \frac{1}{2}(\partial_x F(x + iy) + i\partial_y F(x + iy)),\end{aligned}$$

while derivatives with respect to real variables x, y are denoted $\partial_x F, \partial_y F$ and extended to multi-indices in the usual way:

$$\partial^\alpha := \partial_x^{\alpha_1} \partial_y^{\alpha_2}, \quad \alpha = (\alpha_1, \alpha_2) \in \mathbb{N}_0^2.$$

Directional derivatives are denoted:

$$\partial_v F(z) = v\partial F(z) + \bar{v}\bar{\partial} F(z) = v_1\partial_x F(z) + v_2\partial_y F(z),$$

where $v = v_1 + iv_2 \in \mathbb{C}$ and $|v| = 1$.

Letting $DF(z) \in \mathbb{R}^{2 \times 2}$ be the differential matrix of $F: \mathbb{R}^2 \rightarrow \mathbb{R}^2$, we have the following expressions:

$$(3.1) \quad \det DF(z) = |\partial F(z)|^2 - |\bar{\partial} F(z)|^2 = \operatorname{Im} [\partial_v F(z) \cdot \overline{\partial_{-iv} F(z)}], \quad |v| = 1.$$

We also use the *twisted derivatives* (2.8), which commute with the twisted shifts (1.8):

$$(3.2) \quad (\mathcal{D}_j F_w) = (\mathcal{D}_j F)_w, \quad w \in \mathbb{C}.$$

The *charge* of F at a point $z \in \mathbb{C}$ is

$$\kappa_z = \text{sgn det } DF(z) \in \{-1, 0, 1\}.$$

For a curve $\gamma: [a, b] \rightarrow \mathbb{C}$, $\gamma(t) = x(t) + iy(t)$ the integrals of the forms Fdz and $Fd\bar{z}$ are defined as usual:

$$\begin{aligned} \int_{\gamma} F(z) dz &= \int_a^b F(\gamma(t))(x'(t) + iy'(t)) dt, \\ \int_{\gamma} F(z) d\bar{z} &= \int_a^b F(\gamma(t))(x'(t) - iy'(t)) dt. \end{aligned}$$

We also use the following notation for the *total derivative*:

$$dF = \partial F dz + \bar{\partial} F d\bar{z},$$

and denote by dA the differential of the (Lebesgue) area measure on \mathbb{C} .

Throughout the manuscript we consider the *acquisition lattice* (1.2) with spacing $\delta > 0$ and the *computation domain* (1.1) with side-length $L > 0$. Associated with the grid-spacing δ , we consider the related quantities

$$\delta^* = 2 \lceil \delta^{-1/2}/4 \rceil \delta, \quad \delta^{**} = \lceil \delta^{-1/2} \rceil \delta,$$

which are $\approx \sqrt{\delta}$, and the *coarse grid* (2.1), with spacing δ^* . The restriction of grids to a square are denoted

$$\Lambda_M = \{\lambda \in \Lambda : |\lambda|_{\infty} \leq M\}, \quad \Delta_M = \{\lambda \in \Delta : |\lambda|_{\infty} \leq M\}.$$

In particular, we write $\Lambda_L, \Lambda_{L+\delta}$, etc. for grid points lying on or close to the computation domain (1.1).

3.2. Twisted shifts and Euclidean derivatives. As mentioned, the twisted derivatives (2.8), commute with the twisted shifts (1.8), cf. (3.2). We now observe that for small parameters, Euclidean derivatives and twisted shifts enjoy an approximately Euclidean covariance relation.

Lemma 3.1. *The following holds for a (in the real sense) differentiable function $F: \mathbb{C} \rightarrow \mathbb{C}$:*

$$\begin{aligned} |\partial_x F_{w+w'}(z)| &\leq |w'|_{\infty} |F_w(z+w')| + |\partial_x F_w(z+w')|, & z, w, w' \in \mathbb{C}, \\ |\partial_y F_{w+w'}(z)| &\leq |w'|_{\infty} |F_w(z+w')| + |\partial_y F_w(z+w')|, & z, w, w' \in \mathbb{C}. \end{aligned}$$

Proof. We note that $F_{w+w'}(z) = e^{i\text{Im}(w'\bar{w})} e^{-i\text{Im}(z\bar{w}')} F_w(z+w')$ and compute

$$\begin{aligned} e^{-i\text{Im}(w'\bar{w})} \partial_x F_{w+w'}(z) &= i \text{Im}(w') e^{-i\text{Im}(z\bar{w}')} F_w(z+w') + e^{-i\text{Im}(z\bar{w}')} \partial_x F_w(z+w'), \\ e^{-i\text{Im}(w'\bar{w})} \partial_y F_{w+w'}(z) &= -i \text{Re}(w') e^{-i\text{Im}(z\bar{w}')} F_w(z+w') + e^{-i\text{Im}(z\bar{w}')} \partial_y F_w(z+w'), \end{aligned}$$

from where the estimate follows. □

3.3. The sparse grid. With a slight abuse of language, we define the *sparse grid* as the following subset of Λ_L :

$$(3.3) \quad X_L := \{\mu \in \Lambda_L : |\mu - \lambda|_\infty = \delta^{**} \text{ for some } \lambda \in \Delta\},$$

which consists of all (fine) grid points μ that lie on the boundary boxes $Q_{\delta^{**}}(\lambda)$, $\lambda \in \Delta$; see Figure 4. This set is instrumental in the analysis of Twisted PhaseJumps-coarse because the comparison in Step 1 involves evaluating F on points $\lambda + \mu \in X_{L+\delta^{**}}$, cf. (2.2). We record the following simple facts.

Lemma 3.2. *Let $L \geq 1$, $0 < \delta \leq 1$ and X_L be given by (3.3). Then the cardinality of the sparse grid satisfies*

$$(3.4) \quad \#X_L \leq CL^2\delta^{-3/2},$$

for a universal constant C .

In addition, assume that $\delta < 1/16$. Then given $\xi \in \Omega_L$ and $v \in \mathbb{C}$ with $|v| = 1$, there exists $t \in [2, 4]$ and $\tau \in X_{L+1}$ such that $|\xi + \sqrt{\delta}tv - \tau| < \delta$.

Proof. To prove (3.4), note that if $\lambda \in \Delta$ is such that there exists $\mu \in \Lambda_L$ with $|\mu - \lambda|_\infty = \delta^{**}$, then $|\lambda| \leq L + 2$, so there are at most $\lesssim L^2/\delta$ such points. For each such λ , there are at most $\lesssim \delta^{**}/\delta \asymp \delta^{-1/2}$ points $\mu \in \Lambda$ with $|\mu - \lambda|_\infty = \delta^{**}$. Hence, (3.4) follows from a union bound; see Figure 4.

For the second assertion, note that $|\xi + \sqrt{\delta}tv| < L + 1/4 \cdot 4$ for all $t \in [2, 4]$ and thus $\{\xi + \sqrt{\delta}tv : t \in [2, 4]\} \subset \Omega_{L+1}$. Consider the set of vertical and horizontal segments $M_{L+1} = \{z \in \Omega_{L+1} : |z - \lambda|_\infty = \delta^{**} \text{ for some } \lambda \in \Delta\}$. The points in Δ are spaced δ^* apart and the following shows that $\delta^* < \delta^{**} \leq 2\delta^*$:

$$\begin{aligned} \delta^{**} &\geq \sqrt{\delta} > (\sqrt{\delta}/2 + 2\delta) = 2\delta(\delta^{-1/2}/4 + 1) > \delta^*, \\ \delta^{**} &= \lceil \delta^{-1/2} \rceil \delta \leq 4 \lceil \delta^{-1/2}/4 \rceil \delta = 2\delta^*. \end{aligned}$$

Hence, the distance between consecutive horizontal segments in M_{L+1} is at most δ^* (similarly for vertical segments) and the longest line segment in Ω_{L+1} disjoint of M_{L+1} has length at most $\sqrt{2}\delta^*$. Since

$$(4 - 2)\sqrt{\delta} > \sqrt{2}\sqrt{\delta} > \sqrt{2}\delta^*,$$

the line segment $\{\xi + \sqrt{\delta}tv : t \in [2, 4]\}$ must intersect M_{L+1} , i. e., there exists $t \in [2, 4]$ such that $z := \xi + \sqrt{\delta}tv \in M_{L+1}$. Finally, we choose $\tau \in X_{L+1}$ such that $|z - \tau| < \delta$. (This is possible even if the corners of Ω_{L+1} do not align with the fine grid Λ .) \square

3.4. The short-time Fourier transform as a main example. We now discuss why the short-time Fourier transform of a signal impacted by noise is an instance of the input model. For the formulation, we use the Schwartz class $\mathcal{S}(\mathbb{R})$ and the so-called modulation space $M^\infty(\mathbb{R})$ consisting of distributions with bounded short-time Fourier transform [8]. We also interpret Gaussian white noise as a random distribution (generalized stochastic process) [25], which allows us to calculate its short-time Fourier transform; see [22, Section 6.1], or [7] for a different approach.

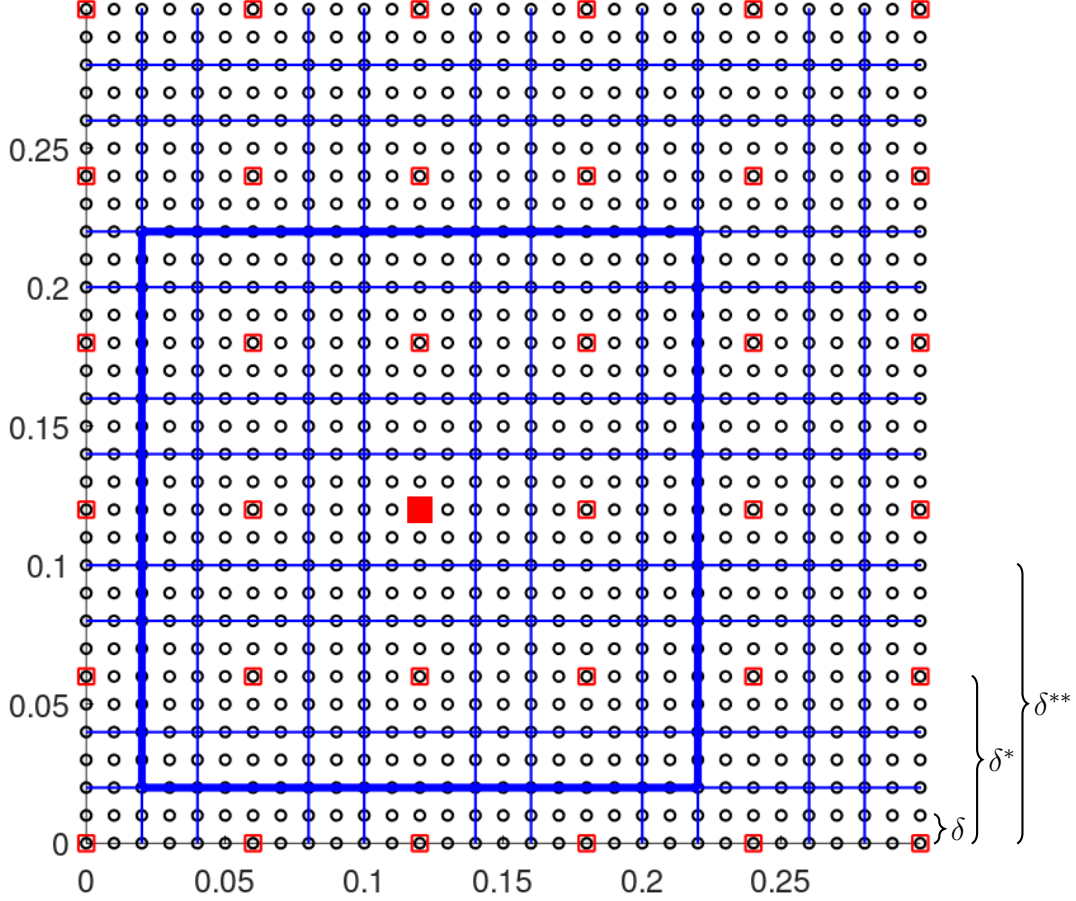


FIGURE 4. Illustration of the different grids. Black circles mark the elements of the fine grid Λ_L , red squares mark the elements of the coarse grid Δ , blue lines mark the set M_{L+1} . The thick blue lines illustrate the part of M_{L+1} originating from the element $\lambda \in \Delta$ highlighted by the filled red square. The illustration is based on $\delta = 1/100$, and thus $\delta^* = 6/100$ and $\delta^{**} = 10/100$.

Lemma 3.3. *Let $g \in \mathcal{S}(\mathbb{R})$ be normalized by $\|g\|_2 = 1$, f^0 standard complex-valued Gaussian white noise, $f^1 \in M^\infty(\mathbb{R})$ and $\sigma > 0$. Set $F = F^1 + \sigma F^0$ with*

$$F^j(z) := e^{-ixy} \cdot V_g f^j(x/\sqrt{\pi}, -y/\sqrt{\pi}), \quad z = x + iy.$$

Then F is almost surely twice continuously differentiable in the real sense, and (2.9), (2.10), (2.11), (2.12), (2.13) hold with $H(x + iy) = e^{-ixy} \cdot V_g g(x/\sqrt{\pi}, -y/\sqrt{\pi})$. In addition, the constant in (2.9) satisfies $A \asymp \|V_g f\|_\infty$.

Proof. This is proved in [22, Lemma 6.1] for the zero mean case and in [15, Lemma 9.2] in full generality. The references only provide bounds for the first order derivatives $\mathcal{D}_1 F^1, \mathcal{D}_2 F^1$ but the same argument applies to second order derivatives $\mathcal{D}_j \mathcal{D}_k F^1$ and shows that $A \asymp \|V_g f\|_\infty$. \square

3.5. Gaussian Weyl-Heisenberg functions. For the remainder of the section, we let $F = F^1 + \sigma F^0$, with $\sigma > 0$, be a random function satisfying the assumptions of Section 2.3, namely: F is almost surely twice continuously differentiable in the real sense, and (2.9), (2.10), (2.11), (2.12), (2.13) hold. This class of random functions was introduced in [22] and further studied in [15]. For short, we say that F is a *Gaussian Weyl-Heisenberg function* (GWHF) with *twisted kernel* H , cf. (2.10).

We note the following symmetry of the twisted kernel H : setting $z = 0$ or $w = 0$ in (2.10) we see that

$$(3.5) \quad H(-z) = \overline{H(z)}, \quad z \in \mathbb{C}.$$

It is important to note the following uniformity property: for arbitrary $w \in \mathbb{C}$, the shifted function $F_w = F_w^0 + \sigma F_w^1$ is another instance of the same stochastic model, with the same twisted kernel H , while the constant A associated to F_w^1 is the same as that associated with F^1 in (2.9).

3.6. Excursion bounds. As a first step, we look into the derivatives of the input function F .

Lemma 3.4. *For multi-indices α, β with $|\alpha|, |\beta| \leq 2$ we have*

$$\text{Cov} [\partial^\alpha F^0(x + iy), \partial^\beta F^0(u + iv)] = \partial_{(x,y)}^\alpha \partial_{(u,v)}^\beta \left[H(z - w) e^{i \text{Im}(z\bar{w})} \right], \quad z = x + iy, w = u + iv \in \mathbb{C}.$$

Proof. Since F is almost surely C^2 , it is a separable Gaussian field. This, together with the fact that $H \in C^6$ allows one to commute expectation and derivatives up to order 2; see [4, Chapter 1] or [1, Section 1.1]. \square

Next, we investigate the typical size of the derivatives of the input function F .

Lemma 3.5. *There exist constants $c, c', C > 0$ that depend on the twisted kernel H such that for every multi-index $|\alpha| \leq 2$, the following excursion bound holds*

$$\mathbb{P} \left(\sup_{|z| \leq 10, |w| \leq L} |\partial^\alpha F_w(z)| > s \right) \leq CL^2 e^{c' \frac{A^2}{\sigma^2}} e^{-c \frac{s^2}{\sigma^2}}, \quad s \geq 0, \quad L \geq 1.$$

Proof. Step 1. Fix a multi-index α with $|\alpha| \leq 2$. We shall apply the Borell–TIS inequality (see e.g., [4, Theorem 2.9] or [1, Theorem 2.1.1]) to the real-valued Gaussian random fields

$$G_1(z) := \text{Re}[\partial^\alpha F^0(z)], \quad G_2(z) := \text{Im}[\partial^\alpha F^0(z)]$$

on the domain $\{z : |z| < 11\}$.

Let us denote $K_j(\xi, \chi) = \mathbb{E}[G_j(\xi) \overline{G_j(\chi)}]$. By Lemma 3.4, for $|\xi|, |\chi| \leq 11$,

$$\text{Var}[G_j(\xi) - G_j(\chi)] = K_j(\xi, \xi) + K_j(\chi, \chi) - 2 \text{Re}[K_j(\xi, \chi)] \lesssim \sup_{|\beta| \leq 5, |z| \leq 22} |\partial^\beta H(z)| \cdot |\xi - \chi|.$$

This estimate allows us to apply Dudley’s inequality because it compares the metric induced by G_j to the usual Euclidean metric, and provides bounds for the corresponding entropy numbers [4, Chapter 2], [1, Chapter 2]. By Dudley’s inequality [4, Theorem 2.10] [1, Theorem 1.3.3], we have the estimate

$$B_j := \mathbb{E} \left[\sup_{|z| \leq 11} G_j(z) \right] \leq C, \quad j = 1, 2,$$

where the constant C depends only on H . Similarly, by Lemma 3.4,

$$\sigma_j^2 := \sup_{|z| \leq 11} \text{Var } G_j(z) \leq C, \quad j = 1, 2,$$

with the constant C depending only on H . By the Borell-TIS inequality (see, e.g., [4, Theorems 2.8 and 2.9]),

$$(3.6) \quad \mathbb{P}\left(\sup_{|z| \leq 11} G_j(z) > s\right) = \mathbb{P}\left(\sup_{|z| \leq 11} G_j(z) - B_j > s - B_j\right) \leq 2e^{-\frac{1}{2}(s-B_j)^2/\sigma_j^2}.$$

Here, we may assume that σ_j is not zero, because otherwise $G_j(z)$ would be almost surely 0 for all $|z| \leq 11$, in which case the excursion bound (3.6) holds trivially. Arguing similarly with $-G_j$ and collecting all estimates, we obtain

$$(3.7) \quad \mathbb{P}\left(\sup_{|z| < 11} |\partial^\alpha F^0(z)| > s\right) \leq C_1 e^{-c_1 s^2}, \quad s \geq 0.$$

Here and for the remainder of the proof C_j, c_j will denote constants that depend only on the twisted kernel H .

Step 2. We now compare Euclidean and twisted derivatives. For an arbitrary $G : \mathbb{C} \rightarrow \mathbb{C}$ that is C^2 in the real sense we define

$$\begin{aligned} \|G\|_* &:= \sup_{|z| \leq 10} \max \{|G(z)|, |\mathcal{D}_j G(z)|, |\mathcal{D}_j \mathcal{D}_i G(z)| : i, j = 1, 2\}, \\ \|G\|_{**} &:= \sup_{|z| \leq 11} \max \{|G(z)|, |\mathcal{D}_j G(z)|, |\mathcal{D}_j \mathcal{D}_i G(z)| : i, j = 1, 2\}. \end{aligned}$$

Then

$$(3.8) \quad \|G\|_* \asymp \sup_{|\alpha| \leq 2} \sup_{|z| \leq 10} |\partial^\alpha G(z)|,$$

where the implied constants are absolute. The advantage of the introduced expressions is that they are naturally compatible with twisted shifts. For example, by the commutation relation (3.2),

$$\begin{aligned} \|(G_{w_1})_{w_2}\|_* &= \sup_{|z| \leq 10} \max_{i,j=1,2} \{|(G_{w_1})_{w_2}(z)|, |((\mathcal{D}_j G)_{w_1})_{w_2}(z)|, |((\mathcal{D}_j \mathcal{D}_i G)_{w_1})_{w_2}(z)|\} \\ &= \sup_{|z| \leq 10} \max_{i,j=1,2} \{|G(z + w_1 + w_2)|, |\mathcal{D}_j G(z + w_1 + w_2)|, |\mathcal{D}_j \mathcal{D}_i G(z + w_1 + w_2)|\} \\ &= \|G_{w_1+w_2}\|_*. \end{aligned}$$

Similarly,

$$(3.9) \quad \sup_{|w| \leq 1} \|G_w\|_* = \sup_{|w| \leq 1} \sup_{|z| \leq 10} \max_{i,j=1,2} \{|G(z+w)|, |\mathcal{D}_j G(z+w)|, |\mathcal{D}_j \mathcal{D}_i G(z+w)|\} = \|G\|_{**}.$$

As a consequence of (3.8), the excursion bounds (3.7) can be summarized as

$$\mathbb{P}(\|F^0\|_{**} > s) \leq C_2 e^{-c_2 s^2}, \quad s \geq 0,$$

while (2.9) and (3.2) imply that $\|F^1\|_{**} \leq A$. Thus,

$$\|F\|_{**} \leq A + \sigma \|F^0\|_{**},$$

and therefore

$$(3.10) \quad \mathbb{P}(\|F\|_{**} > s) \leq \mathbb{P}(\|F^0\|_{**} > (s - A)/\sigma) \leq C_2 e^{-c_2 \frac{(s-A)^2}{\sigma^2}}.$$

Step 3. Finally, we cover the domain Ω_L with $O(L^2)$ translates of the square $[-1, 1]^2$, which we denote $[-1, 1]^2 + \omega_{j,k}^L$. We now make the crucial observation that the functions $F_{\omega_{j,k}^L}$ satisfy the same assumptions as F , with uniform estimates. Hence, we can apply (3.10) to each $F_{\omega_{j,k}^L}$ in lieu of F , and with help from (3.8) and (3.9) bound

$$\begin{aligned} \mathbb{P}\left(\sup_{|z| \leq 10, |w| \leq L} |\partial^\alpha F_w(z)| > s\right) &\leq \sum_{j,k} \mathbb{P}\left(\sup_{|z| \leq 10, |w| \leq 1} |\partial^\alpha F_{w+\omega_{j,k}^L}(z)| > s\right) \\ &\leq \sum_{j,k} \mathbb{P}\left(\sup_{|w| \leq 1} \|F_{w+\omega_{j,k}^L}\|_* > c_4 s\right) = \sum_{j,k} \mathbb{P}\left(\sup_{|w| \leq 1} \|(F_{\omega_{j,k}^L})_w\|_* > c_4 s\right) \\ &= \sum_{j,k} \mathbb{P}\left(\|F_{\omega_{j,k}^L}\|_{**} > c_4 s\right) \leq C_5 L^2 \exp\left[-c_2 \frac{(c_4 s - A)^2}{\sigma^2}\right] \\ &\leq C_5 L^2 \exp\left[-\frac{c_2}{2} \frac{c_4^2 s^2 - 2A^2}{\sigma^2}\right], \end{aligned}$$

where we used that $c_4^2 s^2 = ((c_4 s - A) + A)^2 \leq 2((c_4 s - A)^2 + A^2)$. \square

3.7. The argument principle. We note the following sufficient condition for the accurate calculation of the variation of the complex argument along a curve.

Lemma 3.6 (Unproblematic calculation of argument change). *Let $\tau \in \mathbb{C} \setminus \{0\}$ and $\alpha: [a, b] \rightarrow \mathbb{C}$ continuously differentiable. Suppose that $\operatorname{Re}[\bar{\tau}\alpha(t)] > 0$, for all $t \in [a, b]$. Then*

$$\operatorname{Im} \int_\alpha \frac{dz}{z} = \arg[\alpha(b)\overline{\alpha(a)}].$$

Proof. We assume without loss of generality that $|\tau| = 1$, let \log be the principal branch of the logarithm, and compute

$$\begin{aligned} \operatorname{Im} \int_\alpha \frac{dz}{z} &= \operatorname{Im} \int_{\bar{\tau}\alpha} \frac{dz}{z} = \operatorname{Im} [\log(\bar{\tau}\alpha(b)) - \log(\bar{\tau}\alpha(a))] \\ &= \arg(\bar{\tau}\alpha(b)) - \arg(\bar{\tau}\alpha(a)). \end{aligned}$$

Since $\arg(\bar{\tau}\alpha(b)), \arg(\bar{\tau}\alpha(a)) \in (-\pi/2, \pi/2)$, we have $\arg(\bar{\tau}\alpha(b)) - \arg(\bar{\tau}\alpha(a)) \in (-\pi, \pi)$ and, therefore,

$$\arg(\bar{\tau}\alpha(b)) - \arg(\bar{\tau}\alpha(a)) = \arg[\bar{\tau}\alpha(b)\overline{\bar{\tau}\alpha(a)}] = \arg[\alpha(b)\overline{\alpha(a)}]. \quad \square$$

3.8. Singularity of the covariance matrix. In order to perform smoothed analysis of Twisted PhaseJumps-coarse we will study correlations between F and its derivatives at various points. As a first step, we consider the zero-mean random vector

$$(3.11) \quad (F^0(0), \partial F^0(0), \bar{\partial} F^0(0)).$$

The following lemma shows that the components of (3.11) may exhibit deterministic relations.

Lemma 3.7. *Suppose that $H(z) = e^{-|z|^2/2}$, $z \in \mathbb{C}$, and define $G^0(z) = e^{|z|^2/2}F^0(z)$. Then G^0 is almost surely an entire function, and, as a consequence, almost surely,*

$$(3.12) \quad \bar{\partial}F^0(z) + \frac{z}{2}F^0(z) = 0, \quad z \in \mathbb{C}.$$

In addition $F^0(0)$ and $\partial F^0(0)$ are independent standard complex normal variables.

Proof. We first compute the covariance kernel of the random Gaussian function G^0 :

$$\begin{aligned} \mathbb{E}[G^0(z) \cdot \overline{G^0(w)}] &= e^{|z|^2/2}e^{|w|^2/2}H(z-w)e^{i\text{Im}(z\bar{w})} \\ &= e^{|z|^2/2}e^{|w|^2/2}e^{-|z-w|^2/2}e^{i\text{Im}(z\bar{w})} = e^{z\bar{w}}. \end{aligned}$$

By Lemma 3.4, we can then interchange expectation and differentiation and compute the covariance kernel of $\bar{\partial}G^0$:

$$\mathbb{E}[\bar{\partial}G^0(z) \cdot \overline{\bar{\partial}G^0(w)}] = \mathbb{E}[\bar{\partial}G^0(z) \cdot \overline{\partial G^0(w)}] = \partial_w \bar{\partial}_z e^{z\bar{w}} = 0.$$

Thus $\bar{\partial}G^0$ is almost surely the zero function, G^0 is almost surely entire, and

$$\bar{\partial}F^0(z) = \bar{\partial}[e^{-z\bar{z}/2}G^0(z)] = e^{-|z|^2/2}(\bar{\partial}G^0(z) - \frac{z}{2}G^0(z)) = -\frac{z}{2}F^0(z), \quad z \in \mathbb{C},$$

which proves (3.12).

Similarly,

$$\mathbb{E}[G^0(z) \cdot \overline{\partial G^0(w)}] = \bar{\partial}_w e^{z\bar{w}} = ze^{z\bar{w}},$$

and

$$\mathbb{E}[\partial G^0(z) \cdot \overline{\partial G^0(w)}] = \partial_z \bar{\partial}_w e^{z\bar{w}} = e^{z\bar{w}} + z\bar{w}e^{z\bar{w}}.$$

This shows that the covariance matrix of the Gaussian vector $(F^0(0), \partial F^0(0)) = (G^0(0), \partial G^0(0))$ is the identity, and gives the remaining claim. \square

The function G^0 in Lemma 3.7 is known as a *Gaussian entire function (GEF)* and can also be described as a random Taylor series with adequately normalized independent complex normal coefficients [28, 26]. Motivated by this identification, we say that F is a GWHF with twisted kernel $H(z) = H^{GEF}(z) = e^{-|z|^2/2}$.

In the situation of Lemma 3.7, the vector (3.11) has a singular covariance, as its third component vanishes. The next proposition shows that up to a change of variables, this is the only case in which the components of (3.11) are deterministically related.

Proposition 3.8. *Suppose there exist constants $a, b, c \in \mathbb{C}$ such that, almost surely,*

$$(3.13) \quad aF^0(0) = b\partial F^0(0) + c\bar{\partial}F^0(0).$$

Then $|c|^2 - |b|^2 > 0$ and

$$(3.14) \quad F^0(z) = e^{[-z(\bar{a}c + a\bar{b}) + \bar{z}(\bar{a}b + a\bar{c})]/(|c|^2 - |b|^2)} \cdot F^{GEF}(R(z)),$$

where

$$(3.15) \quad R(z) = (|c|^2 - |b|^2)^{-1/2}(cz - b\bar{z})$$

and F^{GEF} is a zero-mean GWHF with twisted kernel $H^{GEF}(z) := e^{-|z|^2/2}$.

Proof. The deterministic function F^1 plays no role in this proposition, so we will simplify the notation by assuming that $F^1 \equiv 0$ and thus $F = F^0$.

Equation (3.13) can be rewritten in terms of twisted derivatives as

$$aF(0) = b\mathcal{D}_1F(0) + c\mathcal{D}_2F(0).$$

Since the stochastics of F are invariant under twisted shifts, the same relation holds when we replace F by F_z . This implies that, for each $z \in \mathbb{C}$,

$$(3.16) \quad aF(z) = b\mathcal{D}_1F(z) + c\mathcal{D}_2F(z)$$

holds almost surely (where the exceptional event that may depend on z). Multiplying both sides of (3.16) by $\overline{F(0)}$ and taking an expectation yields

$$aH(z) = b\mathcal{D}_1H(z) + c\mathcal{D}_2H(z), \quad z \in \mathbb{C}.$$

This is equivalent with

$$(3.17) \quad (a + b\bar{z}/2 - cz/2)H(z) = b\partial H(z) + c\bar{\partial}H(z), \quad z \in \mathbb{C}.$$

Define

$$G(z) = H(bz + \bar{c}\bar{z})$$

so that by the chain rule

$$\partial G(z) = b\partial H(bz + \bar{c}\bar{z}) + c\bar{\partial}H(bz + \bar{c}\bar{z}).$$

Equation (3.17) can be written in terms of G as

$$(3.18) \quad \partial G(z) = G(z) \left[a + b\frac{\overline{bz + \bar{c}\bar{z}}}{2} - c\frac{bz + \bar{c}\bar{z}}{2} \right] = G(z) \left[a + \frac{|b|^2 - |c|^2}{2}\bar{z} \right].$$

As a consequence of (3.5),

$$G(-z) = \overline{G(z)}, \quad z \in \mathbb{C}.$$

Combining this with (3.18) we obtain

$$(3.19) \quad -\bar{\partial}G(-z) = G(-z) \left[\bar{a} + \bar{b}\frac{bz + \bar{c}\bar{z}}{2} - \bar{c}\frac{\bar{b}\bar{z} + cz}{2} \right].$$

We note that the function

$$\tilde{G}(z) = e^{2i\text{Im}(az) + (|b|^2 - |c|^2)|z|^2/2}, \quad z \in \mathbb{C},$$

also solves (3.18) and (3.19), while $\tilde{G}(0) = 1 = H(0) = G(0)$. Since \tilde{G} is non-vanishing, we can use the PDEs (3.18) and (3.19) to show that $(\partial(G/\tilde{G}), \bar{\partial}(G/\tilde{G})) \equiv (0, 0)$ and conclude that $G \equiv \tilde{G}$, i.e.,

$$(3.20) \quad H(bz + \bar{c}\bar{z}) = e^{2i\text{Im}(az) + (|b|^2 - |c|^2)|z|^2/2}, \quad z \in \mathbb{C}.$$

As a consequence,

$$|H(bz + \bar{c}\bar{z})|^2 = e^{(|b|^2 - |c|^2)|z|^2}, \quad z \in \mathbb{C}.$$

On the other hand, by (2.12) and (2.13), $|H(z)|^2$ has a strict local maximum at $z = 0$, which forces $|c| > |b|$, as claimed.

Let us replace z by $\bar{z}/(|c|^2 - |b|^2)^{1/2}$ in (3.20) to get

$$(3.21) \quad H(M(z)) = e^{-2i\text{Im}(\bar{a}_*z) - |z|^2/2},$$

where

$$M(z) = (|c|^2 - |b|^2)^{-1/2}(\bar{c}z + b\bar{z}) \quad \text{and} \quad a_* = (|c|^2 - |b|^2)^{-1/2}a.$$

The linear map M is *symplectic*, that is,

$$\text{Im}(M(z)\overline{M(w)}) = \text{Im}(z\bar{w}), \quad z, w \in \mathbb{C},$$

so by (3.21) we obtain

$$\begin{aligned} \mathbb{E} \left[e^{2i\text{Im}(\bar{a}_*z)} F(M(z)) \cdot \overline{e^{2i\text{Im}(\bar{a}_*w)} F(M(w))} \right] &= e^{2i\text{Im}(\bar{a}_*(z-w))} H(M(z-w)) e^{i\text{Im}(z\bar{w})} \\ &= e^{-|z-w|^2/2} e^{i\text{Im}(z\bar{w})}. \end{aligned}$$

Hence,

$$(3.22) \quad F^{GEF}(z) := e^{2i\text{Im}(\bar{a}_*z)} F(M(z))$$

is a GWHF with twisted kernel $H^{GEF}(z) := e^{-|z|^2/2}$. (Clearly, almost all realizations of F^{GEF} are C^2 because those of F are.) We note that the inverse transformation of M is (3.15), and (3.22) then yields (3.14). \square

3.9. Zeros and almost multiplicities. We first note that the zeros of F are almost surely non-degenerate.

Lemma 3.9. *The following holds almost surely:*

$$(3.23) \quad \det DF(z) \neq 0, \quad z \in \{F = 0\}.$$

Proof. The claim follows from [4, Proposition 6.5], which requires that F be C^2 almost surely, as we assume, and that the probability density of $F(z)$ be bounded near the origin uniformly on z , which is true because $F(z)$ is a circularly symmetric complex Gaussian vector with variance $\text{Var}[F(z)] = H(0) = 1$ and bounded mean by (2.9). \square

The following proposition gives an analytic expression for the expected charge of a GWHF on a domain, and provides a useful benchmark to numerically test Theorem 2.2.

Proposition 3.10 (First intensity of charged zeros). *Set*

$$(3.24) \quad \rho_1^\pm(z) := \frac{1}{\pi\sigma^2} e^{-|F^1(z)|^2/\sigma^2} \left(|\mathcal{D}_1 F^1(z) - c_1 F^1(z)|^2 - |\mathcal{D}_2 F^1(z) - c_2 F^1(z)|^2 + \sigma^2 \right), \quad z \in \mathbb{C},$$

where $c_1 := \partial H(0)$ and $c_2 := \bar{\partial} H(0)$. Then, for every Borel set $E \subset \mathbb{C}$,

$$\mathbb{E} \left[\sum_{z \in E, F(z)=0} \kappa_z \right] = \int_E \rho_1^\pm(z) dA(z).$$

Similarly, there exists a measurable function $\rho_1 : \mathbb{C} \rightarrow [0, \infty)$ such that

$$(3.25) \quad \mathbb{E}[\#\{z \in E : F(z) = 0\}] = \int_E \rho_1(z) dA(z).$$

As a consequence, if E has null Lebesgue measure, then $\{F = 0\} \cap E = \emptyset$ almost surely.

Proof. To obtain the functions ρ_1 and ρ_1^\pm we shall invoke Kac-Rice's formulae [4, 1]. Specifically, to obtain a measurable function ρ_1 satisfying (3.25), we invoke [4, Theorem 6.2], which requires: (a) F to be almost surely C^1 , which we assume; (b) $\text{Var}[F(z)]$ to be non-zero for all z , which in our case is 1; (c) the non-degeneracy condition (3.23). (The theorem also gives a concrete expression for ρ_1 , which we shall not need.)

For ρ_1^\pm we need a weighted version of Kac-Rice's formula, found in [4, Theorem 6.4], and a routine regularization argument, which can be found in the proof of [22, Lemma 3.3] and we skip. Important for us is that [4, Theorem 6.4] provides the expression,

$$\begin{aligned}
\rho_1^\pm(z) &= \frac{1}{\pi\sigma^2} e^{-|F_1(z)|^2/\sigma^2} \cdot \mathbb{E}[\det DF(z) \mid F(z) = 0] \\
&= \frac{1}{\pi\sigma^2} e^{-|F_1(z)|^2/\sigma^2} \cdot \mathbb{E}[(|\partial F(z)|^2 - |\bar{\partial} F(z)|^2) \mid F(z) = 0] \\
(3.26) \quad &= \frac{1}{\pi\sigma^2} e^{-|F_1(z)|^2/\sigma^2} \cdot \mathbb{E}[(|\mathcal{D}_1 F(z) + \frac{\bar{z}}{2} F(z)|^2 - |\mathcal{D}_2 F(z) - \frac{z}{2} F(z)|^2) \mid F(z) = 0].
\end{aligned}$$

Using Lemma 3.4 and stochastic invariance under twisted shifts, we write

$$c_1 = \mathbb{E}[\mathcal{D}_1 F^0(z) \cdot \overline{F^0(z)}] = \mathbb{E}[\mathcal{D}_1 F^0(0) \cdot \overline{F^0(0)}] = \mathbb{E}[\partial F^0(0) \cdot \overline{F^0(0)}] = \partial H(0),$$

and

$$c_2 = \mathbb{E}[\mathcal{D}_2 F^0(z) \cdot \overline{F^0(z)}] = \mathbb{E}[\mathcal{D}_2 F^0(0) \cdot \overline{F^0(0)}] = \mathbb{E}[\bar{\partial} F^0(0) \cdot \overline{F^0(0)}] = \bar{\partial} H(0).$$

As a consequence of (3.5), we have that

$$(3.27) \quad |c_1|^2 = |c_2|^2.$$

Similarly, direct computation shows that

$$(3.28) \quad \text{Var } \mathcal{D}_1 F(z) = -\Delta H(0) + 1/2, \quad \text{Var } \mathcal{D}_2 F(z) = -\Delta H(0) - 1/2;$$

see [15, Lemma 2.2] for a detailed calculation.

The constants c_j are defined so that $\mathcal{D}_j F^0(z) - c_j F^0(z)$ is independent of F^0 , which facilitates conditioning. (In technical terms, we invoke the so-called *Gaussian regression formula*, see, e.g., [4, Proposition 1.2].) We shall split the conditional expectation in (3.26) into two terms. We first write

$$\begin{aligned}
&\mathbb{E}[|\mathcal{D}_1 F(z) + \frac{\bar{z}}{2} F(z)|^2 \mid F(z) = 0] \\
&= \mathbb{E}[|\mathcal{D}_1 F^1(z) + \sigma(\mathcal{D}_1 F^0(z) - c_1 F^0(z)) + c_1 \sigma F^0(z) + \frac{\bar{z}}{2} F^1(z) + \sigma \frac{\bar{z}}{2} F^0(z)|^2 \mid F^0(z) = -F^1(z)/\sigma].
\end{aligned}$$

Because $\mathcal{D}_1 F^0(z) - c_1 F^0(z)$ and $F^0(z)$ are independent, the previous conditional expectation equals

$$\begin{aligned}
&\mathbb{E}\left[|\mathcal{D}_1 F^1(z) + \sigma(\mathcal{D}_1 F^0(z) - c_1 F^0(z)) - c_1 F^1(z)|^2\right] \\
&= |\mathcal{D}_1 F^1(z) - c_1 F^1(z)|^2 + \sigma^2 \cdot \mathbb{E}|\mathcal{D}_1 F^0(z) - c_1 F^0(z)|^2 \\
&= |\mathcal{D}_1 F^1(z) - c_1 F^1(z)|^2 + \sigma^2 \cdot (\text{Var}(\mathcal{D}_1 F^0(z)) - 2|c_1|^2 + |c_1|^2 \text{Var } F^0(z)) \\
&= |\mathcal{D}_1 F^1(z) - c_1 F^1(z)|^2 + \sigma^2 \cdot \text{Var}(\mathcal{D}_1 F^0(z)) - \sigma^2 |c_1|^2,
\end{aligned}$$

where for the first equality we are using that $\mathcal{D}_1 F^0$ and F^0 are circularly symmetric, zero mean complex Gaussians. For the third equality, we employed: $\text{Var } F^0(z) = H(0) = 1$.

We turn to the second term contributing to (3.26), which is analyzed similarly:

$$\begin{aligned}
& \mathbb{E}\left[|\mathcal{D}_2 F(z) - \frac{z}{2}F(z)|^2 \mid F(z) = 0\right] \\
&= \mathbb{E}\left[\left|\mathcal{D}_2 F^1(z) + \sigma(\mathcal{D}_2 F^0(z) - c_2 F^0(z)) + c_2 \sigma F^0(z) - \frac{z}{2}F^1(z) - \sigma \frac{z}{2}F^0(z)\right|^2 \mid F^0(z) = -F^1(z)/\sigma\right] \\
&= \mathbb{E}\left[\left|\mathcal{D}_2 F^1(z) + \sigma(\mathcal{D}_2 F^0(z) - c_2 F^0(z)) - c_2 F^1(z)\right|^2\right] \\
&= \left|\mathcal{D}_2 F^1(z) - c_2 F^1(z)\right|^2 + \sigma^2 \cdot \mathbb{E}\left|\mathcal{D}_2 F^0(z) - c_2 F^0(z)\right|^2 \\
&= \left|\mathcal{D}_2 F^1(z) - c_2 F^1(z)\right|^2 + \sigma^2 \cdot \text{Var}(\mathcal{D}_2 F^0(z)) - \sigma^2 |c_2|^2.
\end{aligned}$$

Combining all the above steps with (3.27) and (3.28), we obtain

$$\mathbb{E}\left[|\partial F(z)|^2 - |\bar{\partial} F(z)|^2 : F(z) = 0\right] = \left|\mathcal{D}_1 F^1(z) - c_1 F^1(z)\right|^2 - \left|\mathcal{D}_2 F^1(z) - c_2 F^1(z)\right|^2 + \sigma^2. \quad \square$$

Remark 3.11 (Universal equilibrium of charge). When $F^1 \equiv 0$, we have $\rho_1^\pm \equiv \frac{1}{\pi}$, a fact that was also derived in [22, Theorem 1.12], and, interestingly, is *independent of the twisted kernel H* . Remarkably, Proposition 3.10 shows that *the universal equilibrium of charge also holds in the presence of a non-zero mean F^1* , as long as the twisted kernel H is real-valued, a situation that is often encountered in applications. Indeed, when H is real-valued, the identity $\overline{H(z)} = H(-z)$ forces $c_1 = c_2 = 0$, and (3.24) is independent of H .

We now turn attention to those zeros of a GWHF F that are degenerate in the sense that DF is rank-deficient, or approximately so up to a certain numerical tolerance. We estimate the likeliness of encountering such approximate zeros, as they are a source of challenge for Twisted PhaseJumps-coarse.

Proposition 3.12 (Approximately degenerate zeros are unlikely to occur). *Let $\alpha, \beta > 0$ and $0 < \delta \leq 1$. Then the following hold.*

(i) *For each $\lambda \in \mathbb{C}$, the probability that the estimate*

$$(3.29) \quad |F_\lambda(0)| \leq \alpha \quad \text{and} \quad |\det DF_\lambda(0)| \leq \beta$$

holds is at most $\leq C\alpha^2\beta\sigma^{-4}$ where the constant C depends only on the twisted kernel H and not on the mean F^1 .

(ii) *The probability that the estimate (3.29) holds for some $\lambda \in X_L$ is at most $\leq CL^2\alpha^2\beta\sigma^{-4}\delta^{-3/2}$, where X_L is the set (3.3).*

(Here, C is a constant that depends only on the twisted kernel H .)

Proof. We focus on proving part (i). Once this is done, a union bound and (3.4) will yield part (ii). Since the function F^0 is invariant under twisted shifts, it suffices to prove (i) only in the case $\lambda = 0$. We also assume first that $\sigma = 1$. The case of general σ is dealt with in the end. We denote by $\Gamma \in \mathbb{C}^{3 \times 3}$ the covariance matrix of the Gaussian random vector $(F^0(0), \partial F^0(0), \bar{\partial} F^0(0))$.

Step 1. We start with the observation that the set

$$T(u, s) := \{z \in \mathbb{C} : ||z + u|^2 - s| \leq \beta\}, \quad u \in \mathbb{C}, s \in \mathbb{R},$$

has area

$$(3.30) \quad \text{Area}(T(u, s)) \leq 2\pi\beta.$$

For negative s the claim is clear. For $s \geq \beta$, we have

$$\text{Area}(T(u, s)) = \pi(\beta + s) - \pi(s - \beta) = 2\pi\beta,$$

while, for $s < \beta$,

$$\text{Area}(T(u, s)) \leq \pi(\beta + s) \leq 2\pi\beta.$$

So, indeed, (3.30) holds.

Step 2. We start by assuming that Γ is non-singular. We denote by

$$(3.31) \quad (\mu_1, \mu_2, \mu_3) := (F^1(0), \partial F^1(0), \bar{\partial} F^1(0))$$

the mean of the vector $(F(0), \partial F(0), \bar{\partial} F(0))$. Let $a, b > 0$ be numbers such that $a \leq \Gamma(0) \leq b$ in the sense of positive definite matrices. In particular, $\det \Gamma(0) \geq a^3$ and

$$\frac{1}{\det \Gamma} e^{-(z_1, z_2, z_3) \Gamma^{-1}(0) (z_1, z_2, z_3)^*} \leq \frac{1}{a^3} e^{-(|z_1|^2 + |z_2|^2 + |z_3|^2)/b} \leq \frac{1}{a^3} e^{-|z_2|^2/b}, \quad z_1, z_2, z_3 \in \mathbb{C}.$$

Consequently,

$$\begin{aligned} & \mathbb{P}(|F(0)| \leq \alpha, |\det DF(0)| \leq \beta) \\ &= \frac{1}{\pi^3 \det \Gamma} \int_{|\mu_1 + z_1| \leq \alpha, \|\mu_2 + z_2\|^2 - \|\mu_3 + z_3\|^2 \leq \beta} e^{-(z_1, z_2, z_3) \Gamma^{-1}(0) (z_1, z_2, z_3)^*} dA(z_1) dA(z_2) dA(z_3) \\ &\leq \frac{1}{\pi^3 a^3} \int_{|z_1| \leq \alpha} \int_{z_2 \in \mathbb{C}} e^{-|z_2 - \mu_2|^2/b} \int_{\||z_2|^2 - |z_3|^2| \leq \beta} dA(z_3) dA(z_2) dA(z_1) \\ &= \frac{1}{\pi^3 a^3} \text{Area}(B_\alpha(0)) \cdot \int_{z_2 \in \mathbb{C}} e^{-|z_2 - \mu_2|^2/b} \cdot \text{Area}(T(0, |z_2|^2)) dA(z_2) \\ &\leq C \alpha^2 \beta, \end{aligned}$$

for a constant C independent of F^1 . As a consequence, the same estimate also holds if we replace F by F_λ with $\lambda \in \mathbb{C}$.

Step 3. We now address the case in which $(F^0(0), \partial F^0(0), \bar{\partial} F^0(0))$ has a singular covariance. This means that there exist constants a, b, c such that

$$aF^0(0) = b\partial F^0(0) + c\bar{\partial} F^0(0).$$

By Proposition 3.8, we have $|c|^2 - |b|^2 > 0$, so we can normalize the constants so that $|c|^2 - |b|^2 = 1$. By the same Proposition, we have

$$F^0(z) = e^{\bar{a}_* z - a_* \bar{z}} F^{GEF}(cz - b\bar{z}),$$

where F^{GEF} is a GWHF with twisted kernel $H^{GEF}(z) = e^{-|z|^2/2}$ and $a_* = -a\bar{c} - \bar{a}b$. By Lemma 3.7, $\bar{\partial} F^{GEF}(0) = 0$, and therefore the Jacobian determinant of F at the origin is

$$\begin{aligned} \det DF(0) &= |\partial F(0)|^2 - |\bar{\partial} F(0)|^2 \\ &= |\partial F^1(0) + \bar{a}_* F^{GEF}(0) + c\partial F^{GEF}(0)|^2 - |\bar{\partial} F^1(0) - a_* F^{GEF}(0) - b\partial F^{GEF}(0)|^2, \end{aligned}$$

where we used the chain rule for Wirtinger derivatives. The vector $(F^{GEF}(0), \partial F^{GEF}(0))$ is, by Lemma 3.7, standard complex Gaussian, i.e., the entries are independent and $\mathcal{N}_{\mathbb{C}}(0, 1)$ distributed. The density of this Gaussian vector is bounded above by $\frac{1}{\pi^2}$, so we may estimate

$$(3.32) \quad \mathbb{P}(|F(0)| \leq \alpha, |\det DF(0)| \leq \beta) \leq \frac{1}{\pi^2} \int_S dA(z_1) dA(z_2),$$

where

$$S := \{(z_1, z_2) \in \mathbb{C}^2 : |z_1 + \mu_1| \leq \alpha, \left| |\mu_2 + \bar{a}_* z_1 + c z_2|^2 - |\mu_3 - a_* z_1 - b z_2|^2 \right| \leq \beta\}$$

and μ_1, μ_2, μ_3 are defined as in (3.31). Using that $|c|^2 - |b|^2 = 1$, the second inequality in the definition of S can be rewritten as

$$\left| |z_2 + u|^2 + s \right| \leq \beta,$$

where

$$\begin{aligned} u &= u(z_1) = \bar{c}(\mu_2 + \bar{a}_* z_1) + \bar{b}(\mu_3 - a_* z_1), \\ s &= s(z_1) = -|u|^2 + |\mu_2 + \bar{a}_* z_1|^2 - |\mu_3 - a_* z_1|^2. \end{aligned}$$

Recalling (3.32) and (3.30) we conclude:

$$\mathbb{P}(|F(0)| \leq \alpha, |\det DF(0)| \leq \beta) \leq \frac{1}{\pi^2} \int_{|z_1 + \mu_1| \leq \alpha} \int_{z_2 \in T(u(z_1), s(z_1))} dA(z_2) dA(z_1) \leq 2\alpha^2 \beta.$$

Because the previous estimate is independent of F^1 , it also holds if we replace F by F_λ for arbitrary $\lambda \in \mathbb{C}$. We have thus proved the theorem in the case $\sigma = 1$.

Step 4. Finally, we will eliminate the assumption $\sigma = 1$ and deal with the general case $\sigma > 0$. Applying result for $\sigma = 1$ to the function $z \mapsto \frac{1}{\sigma} F^1(z) + F^0(z)$, we obtain

$$\begin{aligned} &\mathbb{P}(|F(0)| \leq \alpha, |\det DF(0)| \leq \beta) \\ &= \mathbb{P}\left(|F^1(0)/\sigma + F^0(0)| \leq \alpha/\sigma, \left|\det D\left(\frac{1}{\sigma} F^1 + F^0\right)(0)\right| \leq \beta/\sigma^2\right) \leq C\alpha^2 \beta/\sigma^4, \end{aligned}$$

where C depends only on the twisted covariance kernel H . □

3.10. Poincaré index. We now note that Poincaré's index formula is applicable to GWHFs; see [15] for a comprehensive study of Poincaré indices of GWHFs and applications to the classification of zeros.

Lemma 3.13. *Let $\Omega \subset \mathbb{C}$ be a square or a disk. Then, almost surely,*

$$(3.33) \quad \int_{\partial\Omega} \frac{dF}{F} = \int_{\partial\Omega} \left(\frac{\partial F}{F} dz + \frac{\bar{\partial} F}{F} d\bar{z} \right) = 2\pi i \sum_{z \in \Omega, F(z)=0} \kappa_z.$$

Proof. Poincaré's index formula (3.33) is valid if (a) F is twice continuously differentiable, as we assume; (b) F does not vanish on $\partial\Omega$; and (c) 0 is a regular value of F ; see, for example, [27, 31]. Condition (c) holds by Lemma 3.9, while condition (b) follows from Lemma 3.10, since $\partial\Omega$ has null Lebesgue measure, and therefore (3.25) shows that $\mathbb{E}[\#\{F = 0\} \cap \partial\Omega] = 0$. □

4. PROOF OF THEOREM 2.2

4.1. Excluding bad events. Since $L \geq 1$, we can choose the constant $C > 0$ in (2.14) so large that the bound on the failure probability becomes trivial for $\delta \geq 1/64$. Hence, we assume without loss of generality that $0 < \delta < 1/64$. As a consequence,

$$\sqrt{\delta} \leq \lceil \delta^{-1/2} \rceil \delta = \delta^{**} \leq 2\sqrt{\delta} \leq 1/4,$$

an estimate that we will use repeatedly without further mention. We will exclude a number of events that have a small probability for small values of δ . It will be convenient to use the notation $\gamma = \eta\sigma$ where $\eta > 0$ is a constant to be fixed shortly, that depends only on the twisted kernel H , cf. (2.10).

We start with the excursion bounds in Lemma 3.5 and consider the constants $c, c', C > 0$ of its statement. Firstly, we invoke Lemma 3.5 with $s = \gamma\sqrt{\log \frac{1}{\delta}}$ and take $\eta \geq c^{-1/2}$ to conclude that

$$(4.1) \quad \sup_{|z| \leq 10, |w| \leq 9L} |\partial^\alpha F_w(z)| \leq \gamma\sqrt{\log \frac{1}{\delta}}, \quad |\alpha| = 1, 2,$$

except on an event of probability at most

$$\begin{aligned} 9^2 CL^2 \exp\left(c' \frac{A^2}{\sigma^2}\right) \exp\left(-c \frac{s^2}{\sigma^2}\right) &= 9^2 CL^2 \exp\left(c' \frac{A^2}{\sigma^2}\right) \exp\left(-c\eta^2 \log \frac{1}{\delta}\right) \\ &\leq 9^2 CL^2 \exp\left(c' \frac{A^2}{\sigma^2}\right) \delta. \end{aligned}$$

(We choose $9L$ in (4.1) because $Q_{L+5}(0) \subset D_{9L}(0)$.) We use (4.1) to bound the error in first order Taylor expansions. By taking η suitably large we further ensure that

$$(4.2) \quad |F_w(z+u) - F_w(u) - \partial F_w(u)z - \bar{\partial} F_w(u)\bar{z}| \leq \gamma\sqrt{\log \frac{1}{\delta}} \cdot |z|^2, \quad |z|, |u| \leq 5, |w|_\infty \leq L+5,$$

$$(4.3) \quad |TF_w(z+u) - TF_w(u)| \leq \gamma\sqrt{\log \frac{1}{\delta}} \cdot |z|, \quad T = \partial_x, \partial_y, \partial, \bar{\partial}, \quad |z|, |u| \leq 5, |w|_\infty \leq L+5.$$

Secondly, we use Proposition 3.12 with

$$\alpha = \eta_0 \gamma \sqrt{\log \frac{1}{\delta}} \delta, \quad \beta = \eta_1 \gamma^2 \log \frac{1}{\delta} \sqrt{\delta}$$

and constants η_0 and η_1 to be fixed, to ensure that

$$(4.4) \quad \text{for all } \lambda \in X_{L+5}: \quad |F_\lambda(0)| \geq \eta_0 \gamma \sqrt{\log \frac{1}{\delta}} \delta \quad \text{or} \quad |\det DF_\lambda(0)| \geq \eta_1 \gamma^2 \log \frac{1}{\delta} \sqrt{\delta}$$

holds, after excluding an event with probability

$$\lesssim \gamma^4 \sigma^{-4} \eta_0^2 \eta_1 L^2 (\log \frac{1}{\delta})^2 \cdot \delta \lesssim \eta^4 \eta_0^2 \eta_1 L^2 (\log \frac{1}{\delta})^2 \cdot \delta.$$

Finally, we exclude certain null-probability events. First, by Lemma 3.10, we can exclude the null-probability event that F vanishes on any grid point $\lambda \in \Lambda$ or on any point of the boundary of the test boxes, i.e., $\partial Q_{\delta^{**}}(\lambda)$, $\lambda \in \Lambda_L$. This implies, in particular, that in Step 2 of the algorithm, $F_\lambda(\mu_j) \neq 0$ and θ_λ is always defined by (2.4). Second, by Lemma 3.9, after excluding a null-probability event, we have

$$(4.5) \quad \det DF_\lambda(z) \neq 0, \quad \text{whenever } F_\lambda(z) = 0 \text{ and } \lambda \in \Lambda.$$

Third, applying Lemma 3.13 to the domain $\Omega = Q_{\delta^{**}}(0)$, we can exclude a null-probability event and ensure that (3.33) holds simultaneously for all functions F_λ , $\lambda \in \Lambda$ in lieu of F .

Altogether, we exclude events with total probability $\lesssim L^2 \cdot (\log \frac{1}{\delta})^2 \cdot \exp(c'A^2/\sigma^2) \cdot \delta$. We now show that under the complementary event, the conclusions of the theorem hold. (To fully specify the failure probability, we need to fix the constants η_0 and η_1 ; for clarity, we do this throughout the proof, by imposing various absolute lower bounds on η_0 and η_1 .)

4.2. The true zeros are adequately separated. We claim that the zero set of F is $7\delta^{**} = 7\lceil\delta^{-1/2}\rceil\delta$ separated (wrt. the infinity norm):

$$(4.6) \quad \inf \{ |\xi - \xi'|_\infty : \xi, \xi' \in \{F = 0\} \cap \Omega_{L+\delta^{**}}, \xi \neq \xi' \} \geq 7\lceil\delta^{-1/2}\rceil\delta.$$

Suppose on the contrary that $F(\xi_1) = F(\xi_2) = 0$, with $\xi_1, \xi_2 \in \Omega_{L+\delta^{**}}$ and

$$0 < |\xi_1 - \xi_2|_\infty < 7\lceil\delta^{-1/2}\rceil\delta.$$

We linearize F_{ξ_1} around 0 and evaluate at $\xi_2 - \xi_1$: by (4.2) with $w = \xi_1$, $u = 0$ and $z = \xi_2 - \xi_1$, we obtain

$$(4.7) \quad |\partial F_{\xi_1}(0)(\xi_2 - \xi_1) + \bar{\partial} F_{\xi_1}(0)\overline{(\xi_2 - \xi_1)}| \leq \gamma\sqrt{\log \frac{1}{\delta}}|\xi_2 - \xi_1|^2.$$

The use of (4.2) is valid because $|\xi_1|_\infty \leq L + \delta^{**} \leq L + 1$ and $|\xi_2 - \xi_1| \leq 7\sqrt{2}\delta^{**} \leq 7\sqrt{2}/4 < 5$, and we also have $|F_{\xi_1}(0)| = |F(\xi_1)| = 0$ and $|F_{\xi_1}(\xi_2 - \xi_1)| = |F(\xi_2)| = 0$.

Let $v := (\xi_2 - \xi_1)/|\xi_2 - \xi_1|$. Regarding v as an element of \mathbb{R}^2 , (4.7) implies

$$(4.8) \quad |DF_{\xi_1}(0) \cdot v| \leq \gamma\sqrt{\log \frac{1}{\delta}}|\xi_2 - \xi_1| \leq 7\sqrt{2}\gamma\sqrt{\log \frac{1}{\delta}}\lceil\delta^{-1/2}\rceil\delta.$$

We now argue that one can move away from ξ_1 along the line with direction v , traveling a distance $\gtrsim \sqrt{\delta}$, and finishing close to the sparse grid X_L . More precisely, we use Lemma 3.2 (with $L + 1$ in lieu of L) to select the point $\xi_3 = \xi_1 + b\sqrt{\delta}v$ with

$$2 \leq b \leq 4,$$

and $\tau \in X_{L+2}$ with

$$(4.9) \quad |\xi_3 - \tau| \leq \delta.$$

By (4.2), we have

$$|F_{\xi_1}(\xi_3 - \xi_1) - \underbrace{F_{\xi_1}(0)}_{=0} - \partial F_{\xi_1}(0)(\xi_3 - \xi_1) - \bar{\partial} F_{\xi_1}(0)\overline{(\xi_3 - \xi_1)}| \leq \gamma\sqrt{\log \frac{1}{\delta}}|\xi_1 - \xi_3|^2 \leq b^2\gamma\sqrt{\log \frac{1}{\delta}}\delta,$$

which, together with (4.8), implies

$$\begin{aligned} |F_{\xi_3}(0)| &= |F_{\xi_1}(\xi_3 - \xi_1)| \\ &\leq b^2\gamma\sqrt{\log \frac{1}{\delta}}\delta + |\partial F_{\xi_1}(0)(\xi_3 - \xi_1) + \bar{\partial} F_{\xi_1}(0)\overline{(\xi_3 - \xi_1)}| \\ &= b^2\gamma\sqrt{\log \frac{1}{\delta}}\delta + |b\sqrt{\delta}DF_{\xi_1}(0) \cdot v| \\ &\leq b^2\gamma\sqrt{\log \frac{1}{\delta}}\delta + 7\sqrt{2}b\gamma\sqrt{\log \frac{1}{\delta}}\lceil\delta^{-1/2}\rceil\delta^{3/2} \\ &\leq (b^2 + 28b)\gamma\sqrt{\log \frac{1}{\delta}}\delta \end{aligned}$$

$$\leq 128\gamma\sqrt{\log \frac{1}{\delta}}.$$

Recall that, by construction, $\tau \in X_{L+2} \subset \Omega_{L+2}$, so we can invoke (4.2) and (4.9) to obtain,

$$(4.10) \quad |F_\tau(\xi_3 - \tau) - F_\tau(0) - \partial F_\tau(0)(\xi_3 - \tau) - \bar{\partial} F_\tau(0)\overline{(\xi_3 - \tau)}| \leq \gamma\sqrt{\log \frac{1}{\delta}}\delta^2.$$

By (4.1), we have

$$(4.11) \quad |\bar{\partial} F_\tau(0)|, |\partial F_\tau(0)| \leq \gamma\sqrt{\log \frac{1}{\delta}}.$$

On the other hand, we have just derived the estimate

$$|F_\tau(\xi_3 - \tau)| = |F_{\xi_3}(0)| \leq 128\gamma\sqrt{\log \frac{1}{\delta}}\delta.$$

Combining this with (4.9), (4.10) and (4.11), we have

$$(4.12) \quad |F_\tau(0)| \leq 128\gamma\sqrt{\log \frac{1}{\delta}}\delta + 2\gamma\sqrt{\log \frac{1}{\delta}}\delta + \gamma\sqrt{\log \frac{1}{\delta}}\delta^2 \leq 131\gamma\sqrt{\log \frac{1}{\delta}}\delta,$$

where we used $\delta \leq 1$. Next, we evaluate the directional derivative from τ towards ξ_1 . Note first that

$$|\tau - \xi_1| \leq |\tau - \xi_3| + |\xi_3 - \xi_1| \leq \delta + b\sqrt{\delta} \leq (b+1)\sqrt{\delta} \leq 5\sqrt{\delta}.$$

By (4.2),

$$|\underbrace{F_\tau(\xi_1 - \tau) - F_\tau(0) - \partial F_\tau(0)(\xi_1 - \tau) - \bar{\partial} F_\tau(0)\overline{(\xi_1 - \tau)}}_{=0}| \leq 25\gamma\sqrt{\log \frac{1}{\delta}}\delta,$$

which, together with (4.12) implies

$$(4.13) \quad |\partial F_\tau(0)(\xi_1 - \tau) + \bar{\partial} F_\tau(0)\overline{(\xi_1 - \tau)}| \leq 156\gamma\sqrt{\log \frac{1}{\delta}}\delta.$$

Second, by (4.9),

$$|\tau - \xi_1| \geq |\xi_3 - \xi_1| - |\tau - \xi_3| \geq b\sqrt{\delta} - \delta \geq \sqrt{\delta},$$

where we used that $b \geq 2$. Set

$$w := (\tau - \xi_1)/|\tau - \xi_1|.$$

Then (4.13) implies that

$$(4.14) \quad |\partial_w F_\tau(0)| = |DF_\tau(0) \cdot w| \leq 156\gamma\sqrt{\log \frac{1}{\delta}}\sqrt{\delta}.$$

On the other hand, (4.1) implies that

$$(4.15) \quad |\partial_{-iw} F_\tau(0)| \leq 2\gamma\sqrt{\log \frac{1}{\delta}}.$$

Combining (4.14) with (4.15) and the expression for $\det DF_\tau(0)$ in (3.1), we obtain

$$|\det DF_\tau(0)| \leq 312\gamma^2 \log \frac{1}{\delta} \sqrt{\delta}.$$

Taking into account (4.12) we conclude the following: under the assumption that (4.6) fails, there exists a sparse grid point $\tau \in X_{L+2}$ such that

$$|F_\tau(0)| \leq C\gamma\sqrt{\log \frac{1}{\delta}} \quad \text{and} \quad |\det DF_\tau(0)| \leq C\gamma^2 \log \frac{1}{\delta} \sqrt{\delta},$$

where C is an absolute constant. This contradicts (4.4) provided that we let the constants η_0 and η_1 be large enough.

4.3. For the points selected in Step 1, the discretely computed change of the argument equals the actual change. We show that for $\lambda \in Z_1$, the number θ_λ , defined in (2.4), is

$$(4.16) \quad 2\pi i \cdot \theta_\lambda = \int_{\partial Q_{\delta^{**}}(0)} \frac{dF_\lambda(z)}{F_\lambda(z)}.$$

Recall that we have excluded the event where F vanishes on any point of $\partial Q_{\delta^{**}}(\lambda)$. We use the notation of Step 2. Let $\alpha_j : [0, 1] \rightarrow \mathbb{C}$, $j = 1, \dots, N$ be the curve

$$\alpha_j(t) := F_\lambda(t\mu_j + (1-t)\mu_{j-1}).$$

The concatenation $\alpha := \alpha_1 * \dots * \alpha_N$ is a (possibly non-injective) parametrization of $F_\lambda(\partial Q_{\delta^{**}}(0))$, where $\partial Q_{\delta^{**}}(0)$ is parametrized anticlockwise. Thus,

$$i \sum_{j=1}^N \operatorname{Im} \int_{\alpha_j} \frac{dz}{z} = i \operatorname{Im} \int_\alpha \frac{dz}{z} = \int_\alpha \frac{dz}{z} = \int_{\partial Q_{\delta^{**}}(0)} \frac{dF_\lambda(z)}{F_\lambda(z)}.$$

Inspecting the definition (2.4), it suffices to show that

$$\operatorname{Im} \int_{\alpha_j} \frac{dz}{z} = \arg [F_\lambda(\mu_j) \overline{F_\lambda(\mu_{j-1})}], \quad j = 1, \dots, N.$$

To this end, we fix $j \in \{1, \dots, N\}$ and invoke Lemma 3.6 with $\tau = F_\lambda(\mu_{j-1})$. This is possible because we have excluded the event where F_λ vanishes on $\partial Q_{\delta^{**}}(0)$. It suffices to check that

$$(4.17) \quad \operatorname{Re} [F_\lambda(t\mu_j + (1-t)\mu_{j-1}) \overline{F_\lambda(\mu_{j-1})}] > 0, \quad t \in [0, 1].$$

The segment determined by μ_{j-1} and μ_j is either vertical or horizontal. Without loss of generality we assume that it is horizontal: $\operatorname{Im} \mu_{j-1} = \operatorname{Im} \mu_j$. Let $t \in [0, 1]$. We invoke (4.2) with $w = \lambda$ and

$$z_t = t(\mu_j - \mu_{j-1}),$$

which is allowed because $|z_t| \leq \delta \leq 1$ and $\lambda \in \Lambda_L$. Since $z_t \in \mathbb{R}$, the linearization estimate reads

$$(4.18) \quad |F_\lambda(\mu_{j-1} + z_t) - F_\lambda(\mu_{j-1}) - \partial_x F_\lambda(\mu_{j-1}) z_t| \leq \gamma \sqrt{\log \frac{1}{\delta}} |z_t|^2, \quad t \in [0, 1],$$

and, by (4.3),

$$|\partial_x F_\lambda(\mu_{j-1} + u) - \partial_x F_\lambda(\mu_{j-1})| \leq \gamma \sqrt{\log \frac{1}{\delta}} |u|, \quad |u| < 1.$$

In the current notation, the fact that λ passed the algorithm's selection step (Step 1) gives

$$2|F_\lambda(\mu_{j-1}) - F_\lambda(\mu_j)| \leq |F_\lambda(\mu_{j-1})|.$$

Since $|z_1| = \delta$, the previous estimate, together with (4.18) gives

$$(4.19) \quad \begin{aligned} \delta |\partial_x F_\lambda(\mu_{j-1})| &\leq |F_\lambda(\mu_{j-1}) - F_\lambda(\mu_j)| + |F_\lambda(\mu_j) - F_\lambda(\mu_{j-1}) - \partial_x F_\lambda(\mu_{j-1}) z_1| \\ &\leq \frac{1}{2} |F_\lambda(\mu_{j-1})| + \gamma \sqrt{\log \frac{1}{\delta}} \delta^2. \end{aligned}$$

We claim that

$$(4.20) \quad \frac{1}{2}|F_\lambda(\mu_{j-1})| > 2\gamma\sqrt{\log \frac{1}{\delta}}\delta^2.$$

Suppose not, that is,

$$(4.21) \quad |F_\lambda(\mu_{j-1})| \leq 4\gamma\sqrt{\log \frac{1}{\delta}}\delta^2.$$

Then (4.19) yields $|\partial_x F_\lambda(\mu_{j-1})| \leq 3\gamma\sqrt{\log \frac{1}{\delta}}\delta$. By Lemma 3.1 and (4.21),

$$\begin{aligned} |\partial_x F_{\lambda+\mu_{j-1}}(0)| &\leq |\mu_{j-1}|_\infty \cdot |F_\lambda(\mu_{j-1})| + |\partial_x F_\lambda(\mu_{j-1})| \\ &\leq \delta^{**} 4\gamma\sqrt{\log \frac{1}{\delta}}\delta^2 + 3\gamma\sqrt{\log \frac{1}{\delta}}\delta \leq 7\gamma\sqrt{\log \frac{1}{\delta}}\delta, \end{aligned}$$

while, by (4.1), $|\partial_y F_{\lambda+\mu_{j-1}}(0)| \leq \gamma\sqrt{\log \frac{1}{\delta}}$. Consequently

$$(4.22) \quad |\det DF_{\lambda+\mu_{j-1}}(0)| \leq |\partial_x F_{\lambda+\mu_{j-1}}(0)| \cdot |\partial_y F_{\lambda+\mu_{j-1}}(0)| \leq 7\gamma^2 \log \frac{1}{\delta} \leq 7\gamma^2 \log \frac{1}{\delta} \sqrt{\delta},$$

cf. (3.1). In addition, using again (4.21),

$$(4.23) \quad |F_{\lambda+\mu_{j-1}}(0)| = |F_\lambda(\mu_{j-1})| \leq 4\gamma\sqrt{\log \frac{1}{\delta}}\delta^2 \leq 4\gamma\sqrt{\log \frac{1}{\delta}}\delta.$$

The combination of (4.22) and (4.23) contradicts (4.4) provided that the constants η_0 and η_1 are chosen large enough. (Note that in the last bounds we gave up factors of order $\sqrt{\delta}$ and δ ; however other parts of our argument do not allow us to make use of this.)

Hence we conclude that (4.20) holds. We now combine (4.18), (4.19) and (4.20) to estimate

$$\begin{aligned} |F_\lambda(\mu_{j-1} + z_t) - F_\lambda(\mu_{j-1})| &\leq |F_\lambda(\mu_{j-1} + z_t) - F_\lambda(\mu_{j-1}) - \partial_x F_\lambda(\mu_{j-1})z_t| + |z_t| |\partial_x F_\lambda(\mu_{j-1})| \\ &\leq \gamma\sqrt{\log \frac{1}{\delta}}|z_t|^2 + \delta |\partial_x F_\lambda(\mu_{j-1})| \\ &\leq \gamma\sqrt{\log \frac{1}{\delta}}\delta^2 + \frac{1}{2}|F_\lambda(\mu_{j-1})| + \gamma\sqrt{\log \frac{1}{\delta}}\delta^2 \\ &< |F_\lambda(\mu_{j-1})|. \end{aligned}$$

Taking squares yields

$$\begin{aligned} |F_\lambda(\mu_{j-1})|^2 &> |F_\lambda(\mu_{j-1} + z_t) - F_\lambda(\mu_{j-1})|^2 \\ &= |F_\lambda(\mu_{j-1} + z_t)|^2 + |F_\lambda(\mu_{j-1})|^2 - 2 \operatorname{Re} [F_\lambda(\mu_{j-1} + z_t) \overline{F_\lambda(\mu_{j-1})}], \end{aligned}$$

and so $\operatorname{Re} [F_\lambda(\mu_{j-1} + z_t) \overline{F_\lambda(\mu_{j-1})}] > \frac{1}{2}|F_\lambda(\mu_{j-1} + z_t)|^2 > 0$, because we F_λ does not vanish on $\partial Q_{\delta^{**}}(\lambda)$. This gives (4.17) and concludes the proof of (4.16).

4.4. Each true zero is close to a grid point selected in Step 1. We show that

$$(4.24) \quad \{F = 0\} \cap \Omega_L \subset Z_1 + Q_{\lceil \frac{1}{4}\delta^{-1/2} \rceil \delta}(0).$$

Let $\zeta \in \{F = 0\} \cap \Omega_L$ and $\lambda \in \Delta_L$ be such that $|\lambda - \zeta|_\infty \leq \lceil \frac{1}{4}\delta^{-1/2} \rceil \delta = \frac{1}{2}\delta^*$ (The assumption that $L/\delta^* \in \mathbb{N}$ is important here, so as to be able to choose an adequate λ with $|\lambda| \leq L$, even if ζ is close to the boundary of Ω_L .) Let us show that λ passes the test in Step 1. Specifically, let $\mu, \mu' \in \Lambda$ with (2.3) and let us show that (2.2) holds. Note that $\lambda + \mu, \lambda + \mu' \in X_{L+1}$.

As for the right-hand side of (2.2), by (4.1), we have

$$(4.25) \quad \begin{aligned} |F_\lambda(\mu) - F_\lambda(\mu')| &\leq \max \left\{ \sup_{|w| \leq 1} |\partial F_\lambda(w)|, \sup_{|w| \leq 1} |\bar{\partial} F_\lambda(w)| \right\} |\mu - \mu'| \\ &\leq \gamma \delta \sqrt{\log \frac{1}{\delta}}. \end{aligned}$$

To prove (2.2), we distinguish two cases.

Suppose first that $|\det DF_{\lambda+\mu}(0)| < \eta_1 \sqrt{\delta} \gamma^2 \log \frac{1}{\delta}$. Since $\lambda + \mu \in X_{L+1}$, by (4.4),

$$|F_\lambda(\mu)| = |F_{\lambda+\mu}(0)| \geq \eta_0 \gamma \delta \sqrt{\log \frac{1}{\delta}}.$$

Comparing this to (4.25) we obtain

$$|F_\lambda(\mu)| \geq \eta_0 |F_\lambda(\mu) - F_\lambda(\mu')|.$$

Thus (2.2) holds, provided that $\eta_0 \geq 2$.

Suppose now that

$$(4.26) \quad |\det DF_{\lambda+\mu}(0)| \geq \eta_1 \sqrt{\delta} \gamma^2 \log \frac{1}{\delta},$$

and consider the following estimates on the displacement $\zeta - (\lambda + \mu)$:

$$(4.27) \quad |\zeta - (\lambda + \mu)| \leq |\mu| + |\zeta - \lambda| \leq \sqrt{2} \lceil \delta^{-1/2} \rceil \delta + \sqrt{2} \lceil \delta^{-1/2} / 4 \rceil \delta \leq \left(2\sqrt{2} + \frac{\sqrt{2}}{2} \right) \sqrt{\delta},$$

$$(4.28) \quad |\zeta - (\lambda + \mu)| \geq |\mu| - |\zeta - \lambda| \geq \lceil \delta^{-1/2} \rceil \delta - \frac{\sqrt{2}}{2} \delta^{1/2} \geq \left(1 - \frac{\sqrt{2}}{2} \right) \sqrt{\delta}.$$

(Here, we used that $\lceil \delta^{-1/2} / 4 \rceil \leq \delta^{-1/2} / 4 + 1 \leq \delta^{-1/2} / 2$, because $\delta < 1/16$.)

Let $v := \lceil \zeta - (\lambda + \mu) \rceil / |\zeta - (\lambda + \mu)|$. The expression for $\det DF_{\lambda+\mu}(0)$ in (3.1), together with (4.26) and (4.1) give

$$\begin{aligned} \eta_1 \sqrt{\delta} \gamma^2 \log \frac{1}{\delta} &\leq |\det DF_{\lambda+\mu}(0)| \leq |\partial_v F_{\lambda+\mu}(0)| \cdot |\partial_{-iv} F_{\lambda+\mu}(0)| \\ &\leq C^{-1} \gamma \sqrt{\log \frac{1}{\delta}} \cdot |\partial_v F_{\lambda+\mu}(0)|, \end{aligned}$$

for an absolute constant $C > 0$. Consequently

$$(4.29) \quad |\partial_v F_{\lambda+\mu}(0)| \geq C \gamma \eta_1 \sqrt{\delta} \sqrt{\log \frac{1}{\delta}}.$$

On the other hand, since $|F_{\lambda+\mu}(\zeta - (\lambda + \mu))| = |F(\zeta)| = 0$, (4.2) gives

$$\begin{aligned} |F_\lambda(\mu)| &= |F_{\lambda+\mu}(0)| = |F_{\lambda+\mu}(0) - F_{\lambda+\mu}(\zeta - (\lambda + \mu))| \\ &\geq |\partial F_{\lambda+\mu}(0)(\zeta - (\lambda + \mu)) + \bar{\partial} F_{\lambda+\mu}(0)(\overline{\zeta - (\lambda + \mu)})| - \gamma \sqrt{\log \frac{1}{\delta}} \cdot |\zeta - (\lambda + \mu)|^2 \\ &= |\partial_v F_{\lambda+\mu}(0)| \cdot |\zeta - (\lambda + \mu)| - \gamma \sqrt{\log \frac{1}{\delta}} \cdot |\zeta - (\lambda + \mu)|^2. \end{aligned}$$

Further applying (4.29), (4.27) and (4.28) gives

$$\begin{aligned} |F_\lambda(\mu)| &\geq C \gamma \eta_1 \sqrt{\delta} \sqrt{\log \frac{1}{\delta}} \left(1 - \frac{\sqrt{2}}{2} \right) \sqrt{\delta} - \gamma \sqrt{\log \frac{1}{\delta}} \cdot \left(2\sqrt{2} + \frac{\sqrt{2}}{2} \right)^2 \delta \\ &= \left[C \eta_1 \left(1 - \frac{\sqrt{2}}{2} \right) - \left(2\sqrt{2} + \frac{\sqrt{2}}{2} \right)^2 \right] \gamma \sqrt{\log \frac{1}{\delta}} \delta. \end{aligned}$$

Comparing this to (4.25) we obtain

$$|F_\lambda(\mu)| \geq [C\eta_1(1 - \frac{\sqrt{2}}{2}) - (2\sqrt{2} + \frac{\sqrt{2}}{2})^2] |F_\lambda(\mu) - F_\lambda(\mu')|.$$

Therefore, (2.2) holds, provided that η_1 is chosen large enough.

In summary, we conclude that $\lambda \in Z_1$ and, since $|\lambda - \zeta|_\infty \leq \lceil \frac{1}{4}\delta^{-1/2} \rceil \delta$, we have that $\zeta \in Z_1 + Q_{\lceil \frac{1}{4}\delta^{-1/2} \rceil \delta}(0)$. Hence, (4.24) holds, as claimed.

4.5. Winding numbers compute charges. We show the following: for every $\zeta \in \{F = 0\} \cap \Omega_L$ and every $\lambda \in Z_1$ with $|\lambda - \zeta|_\infty \leq \delta^{**}$ we have

$$(4.30) \quad \theta_\lambda = \kappa_\zeta \in \{-1, 1\}.$$

Let $\zeta \in \{F = 0\} \cap \Omega_L$ and $\lambda \in Z_1$ with $|\lambda - \zeta|_\infty \leq \delta^{**}$. Note that we must actually have $|\lambda - \zeta|_\infty < \delta^{**}$ because we have excluded the event where F vanishes on $\partial Q_{\delta^{**}}(\lambda)$.

The box $Q_{\delta^{**}}(0)$ contains at least one zero of F_λ , namely $\zeta - \lambda$, and no other zeros due to (4.6), as, indeed, $\text{diam } Q_{\delta^{**}}(\lambda) = 2\sqrt{2}\lceil \delta^{-1/2} \rceil \delta < 7\lceil \delta^{-1/2} \rceil \delta$ and $Q_{\delta^{**}}(\lambda) \subset \Omega_{L+\lceil \delta^{-1/2} \rceil \delta}$. In addition, recall that we have excluded the event that F_λ has multiple zeros, cf. (4.5). Therefore, by Poincaré's index formula (3.33), the winding number satisfies

$$(4.31) \quad \frac{1}{2\pi i} \int_{\partial Q_{\delta^{**}}(0)} \frac{dF_\lambda}{F_\lambda} = \text{sgn det } DF_\lambda(\zeta - \lambda) \in \{-1, 1\}.$$

On the other hand, since $\lambda \in Z_1$, (4.16) shows that winding number (4.31) is precisely θ_λ . By definition, $\kappa_\zeta = \text{sgn det } DF(\zeta)$. To complete the proof of (4.30), we show that $\text{det } DF_\lambda(\zeta - \lambda) = \text{det } DF(\zeta)$.

Denoting $\lambda = a + ib$ and $z = x + iy$, then $F_\lambda(z) = e^{i(bx-ay)} F(z + \lambda)$ and

$$\begin{aligned} \partial_x F_\lambda(z) &= e^{i(bx-ay)} [\partial_x F(z + \lambda) + ibF(z + \lambda)], \\ \partial_y F_\lambda(z) &= e^{i(bx-ay)} [\partial_y F(z + \lambda) - iaF(z + \lambda)]. \end{aligned}$$

Thus, using the expression in (3.1),

$$\text{det } DF_\lambda(\zeta - \lambda) = -\text{Im} [\partial_x F_\lambda(\zeta - \lambda) \cdot \overline{\partial_y F_\lambda(\zeta - \lambda)}] = -\text{Im} [\partial_x F(\zeta) \cdot \overline{\partial_y F(\zeta)}] = \text{det } DF(\zeta),$$

as claimed.

4.6. After Step 2, each true zero is close to a computed zero. We show that

$$(4.32) \quad \{F = 0\} \cap \Omega_L \subset Z_2 + Q_{\lceil \frac{1}{4}\delta^{-1/2} \rceil \delta}(0).$$

Let $\zeta \in \{F = 0\} \cap \Omega_L$. By (4.24), there exists $\lambda \in Z_1$ such that $|\lambda - \zeta|_\infty \leq \lceil \frac{1}{4}\delta^{-1/2} \rceil \delta$. By (4.30), $\theta_\lambda \neq 0$. This means that $\lambda \in Z_2$ and shows that $\zeta \in Q_{\lceil \frac{1}{4}\delta^{-1/2} \rceil \delta}(\lambda) \subset Z_2 + Q_{\lceil \frac{1}{4}\delta^{-1/2} \rceil \delta}$.

4.7. After Step 2, each computed zero is close to a true zero. We show that

$$(4.33) \quad Z_2 \subset \{F = 0\} + Q_{\lceil \delta^{-1/2} \rceil \delta}.$$

Let $\lambda \in Z_2$. This means that $\lambda \in Z_1$ and $\theta_\lambda \neq 0$. By (4.16), the winding number (4.31) is non-zero. So, by Poincaré's index formula (3.33), F_λ must vanish at some point $\zeta \in Q_{\delta^{**}}(0)$. Since $\lambda + \zeta \in \{F = 0\}$, this proves (4.33).

4.8. Definition of the parametrization. We now look into the sieving step and analyze the final output set Z . The following argument is similar to the one in [14] and is repeated for completeness.

Given $\zeta \in \{F = 0\} \cap \Omega_L$ we claim that there exists $\lambda \in Z$ such that $|\zeta - \lambda|_\infty \leq \delta^{**}$. Suppose to the contrary that

$$(4.34) \quad |\zeta - \mu|_\infty > \delta^{**}, \quad \mu \in Z.$$

By (4.32), there exists $\lambda \in Z_2$ such that $|\zeta - \lambda|_\infty \leq \lceil \frac{1}{4}\delta^{-1/2} \rceil \delta \leq \delta^{**}$. By (4.34), $Z \subsetneq Z \cup \{\lambda\}$. We claim that $Z \cup \{\lambda\}$ is $5\delta^{**}$ -separated with respect to $|\cdot|_\infty$. Since, by construction, Z is $5\delta^{**}$ -separated with respect to $|\cdot|_\infty$, it is enough to check that

$$|\mu - \lambda|_\infty \geq 5\delta^{**}, \quad \mu \in Z.$$

If $\mu \in Z$, by (4.33), there exist $\zeta' \in \{F = 0\}$ such that $|\zeta' - \mu|_\infty \leq \delta^{**}$. If $\zeta' = \zeta$, then $|\zeta - \mu|_\infty \leq \delta^{**}$, contradicting (4.34). Thus $\zeta \neq \zeta'$, while, $\zeta' \in Z + Q_{\delta^{**}}(0) \subset \Omega_{L+\delta^{**}}$. Hence, we are allowed to use (4.6) to conclude that

$$|\mu - \lambda|_\infty \geq |\zeta - \zeta'|_\infty - |\lambda - \zeta|_\infty - |\mu - \zeta'|_\infty \geq 7\delta^{**} - \delta^{**} - \delta^{**} = 5\delta^{**}.$$

In conclusion, the set $Z \cup \{\lambda\}$ is $5\delta^{**}$ -separated:

$$\inf \{|\mu - \mu'|_\infty : \mu, \mu' \in Z \cup \{\lambda\}, \mu \neq \mu'\} \geq 5\delta^{**},$$

which contradicts the maximality of Z . Thus, a point $\lambda \in Z$ such that $|\zeta - \lambda|_\infty \leq \delta^{**}$ must indeed exist. We choose any such point, and define $\Phi(\zeta) = \lambda$.

4.9. Properties of the parametrization. By construction, the map Φ satisfies

$$(4.35) \quad |\Phi(\zeta) - \zeta|_\infty \leq \delta^{**} \leq 2\sqrt{\delta},$$

and therefore (2.15) is proved.

Let us show that $\Phi : \{F = 0\} \cap \Omega_L \rightarrow Z$ is injective. Assume that $\Phi(\zeta) = \Phi(\zeta')$. Then, by (4.35),

$$|\zeta - \zeta'|_\infty \leq |\Phi(\zeta) - \zeta|_\infty + |\Phi(\zeta') - \zeta'|_\infty \leq 2\delta^{**},$$

so the separation bound (4.6) implies that $\zeta = \zeta'$.

We now show that each numerical zero that is away from the boundary is in the image of Φ . Assume that $\lambda \in Z \cap \Omega_{L-\delta^{**}}$ and use (4.33) to select a zero $\zeta \in \{F = 0\}$ such that $|\zeta - \lambda|_\infty \leq \delta^{**}$. Then $\zeta \in \Omega_L$, and, by (4.35),

$$|\Phi(\zeta) - \lambda|_\infty \leq |\Phi(\zeta) - \zeta|_\infty + |\zeta - \lambda|_\infty \leq 2\delta^{**}.$$

As $\lambda, \Phi(\zeta) \in Z$ and Z is $5\delta^{**}$ -separated with respect to $|\cdot|_\infty$ by construction, cf. (2.5), we conclude that $\lambda = \Phi(\zeta)$.

Finally, we note that winding numbers are accurately computed. Given $\zeta \in \{F = 0\} \cap \Omega_L$, we denote $\lambda := \Phi(\zeta)$. By (4.35), ζ and λ are as in the claim in Section 4.5, which gives (2.16).

This concludes the proof of Theorem 2.2. \square

5. NUMERICAL EVALUATION

We proceed to test Twisted PhaseJumps on synthetic signals and assess its effectiveness in computing zeros of the short-time Fourier transform. We also illustrate numerically the advantage of using twisted shifts in this application, and provide numerical support for Theorem 2.2.

5.1. Simulation of the input model. The first step is to simulate the grid values of a function from the input model described in Section 2.3. In principle, this could be done by simulating a large Gaussian vector corresponding to all the samples of the input function on the finite grid (2.1). To speed up computations, we introduce a fast method that amounts to an approximate low-rank factorization of the corresponding covariance matrix. Concretely, we consider the relation (1.11) and discretize the signal $f = f^1 + \sigma f^0$, with $f^1: \mathbb{R} \rightarrow \mathbb{C}$, and f^0 complex Gaussian white noise. We approximate

$$\begin{aligned} F(\sqrt{\pi}u - i\sqrt{\pi}v) &= e^{i\pi uv} \int_{\mathbb{R}} f(t) \overline{g(t-u)} e^{-2\pi i vt} dt \\ &\approx e^{i\pi uv} \sum_{t \in \mathbb{Z}} \int_{[t\delta, (t+1)\delta)} f(s) ds \cdot \overline{g(\delta t - u)} e^{-2\pi i v \delta t} \\ &\approx e^{i\pi uv} \sum_{t \in \mathbb{Z}} \delta[f^1(t\delta) + \xi_t] \cdot \overline{g(\delta t - u)} e^{-2\pi i v \delta t}, \end{aligned}$$

where $\xi_t, t \in \mathbb{Z}$ are independent standard complex normal variables. Second, we fix a domain length L , a lattice spacing δ with $L/\delta \in \mathbb{N}$, and let g^L be the $\frac{1}{2L}$ periodic function that agrees with g on $[-L, L]$. Consider a lattice point $\lambda = \delta k + i\delta j \in \Lambda_L$, set $u = \frac{\delta k}{\sqrt{\pi}}$, $v = \frac{-\delta j}{\sqrt{\pi}}$ above and let us further approximate

$$\begin{aligned} F(\delta k + i\delta j) &\approx e^{i\delta^2 kj} \sum_{t \in \mathbb{Z}} \delta[f^1(t\delta) + \xi_t] \cdot \overline{g(\delta(t - k/\sqrt{\pi}))} e^{2\sqrt{\pi}i\delta t} \\ &\approx e^{i\delta^2 kj} \sum_{t=0}^{2L/\delta-1} \delta[f^1(t\delta) + \xi_t] \cdot \overline{g^L(\delta(t - k/\sqrt{\pi}))} e^{2\sqrt{\pi}i\delta t} =: c_{j,k}. \end{aligned}$$

When g decays fast and L/δ is moderately large, the effect of the last truncation is very mild (and standard practice in Gabor analysis). To approximately simulate input functions F at grid points $\lambda = \delta k + i\delta j$, we simply simulate the vector $(c_{j,k})_{j,k=-L/\delta, \dots, L/\delta}$. See [14, Section 5.1] for additional support for these approximations. We carried out the computations with GNU Octave [13] and the LTFAT toolbox [29].

5.2. Experiments. First, we consider the setting of the STFT of complex white noise using as window function the first Hermite function $g(t) = te^{-t^2/2}$ (normalization is immaterial for our considerations). For this window, the expected charge and number of zeros is available in [22, Corollary 1.10 and 1.13], which provides a useful benchmark. Our experiment shows that, despite missing theoretical guarantees, the Twisted PhaseJumps algorithm performs better than the Twisted PhaseJumps-coarse algorithm for larger values of δ , and gives satisfactory results already at moderate data resolution. In a second example, we show that also when adding a deterministic signal, the simulations using Twisted PhaseJumps conform with the theoretical predictions of the expected charge (Proposition 3.10).

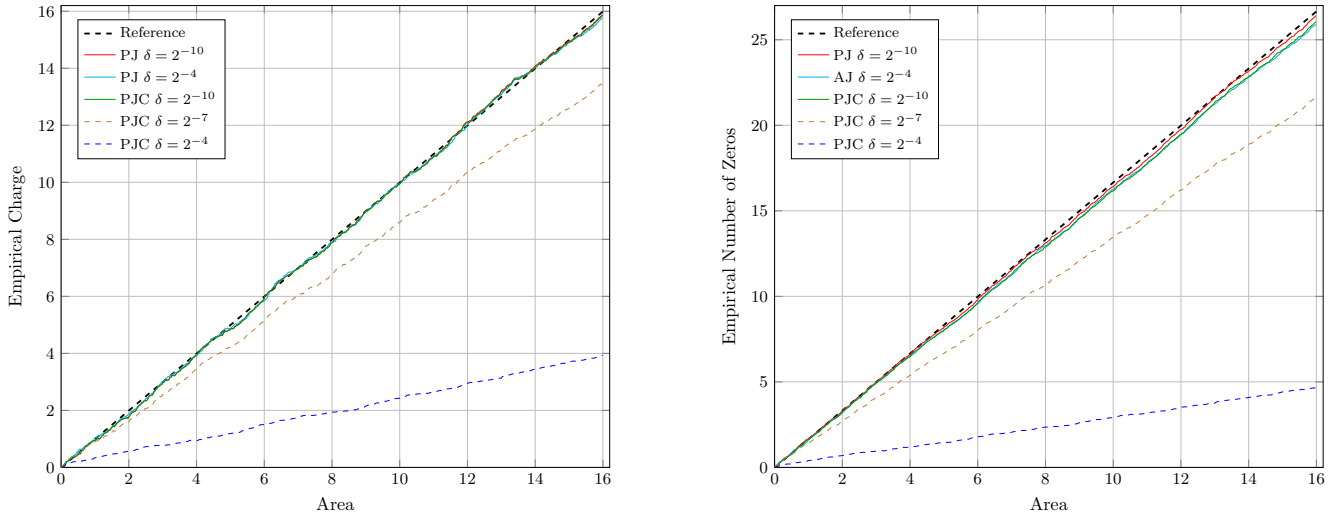


FIGURE 5. Empirical charge (left) and number of zeros (right) based on 100 simulations of the STFT of complex white noise with first Hermite window $g(t) = te^{-t^2/2}$, using the algorithms Twisted PhaseJumps (PJ) and Twisted PhaseJumps-coarse (PJC) for different values of δ .

As a third example, we illustrate the practical role of the phase stabilizing factors in PhaseJumps: although, in theory, the criteria to compute zeros and charges are unaffected by the multiplicative phase term in (1.8), we illustrate that, in the context of the short-time Fourier transform sampled on grids, rapid phase changes render the non-stabilized version of PhaseJumps impractical.

5.3. Experiment 1. We use Twisted PhaseJumps and Twisted PhaseJumps-coarse to calculate the zero set and charges of 100 realizations of the STFT of complex white noise, using the window function $g(t) = te^{-t^2/2}$, and simulated as explained above. The simulations are performed with a small value of the grid spacing parameter $\delta_{\min} = 2^{-10}$ on the square $[-4, 4]^2$, but only zeros in $[-2, 2]^2$ are used, so as to minimize boundary effects. To analyze the dependency on δ , we subsample the fine grid using $\delta = 2^n \delta_{\min}$ for $n = 0, \dots, 6$. In Fig. 5, we show the computed charge and number of zeros for selected values of δ within an ever increasing domain and compare the results with ensemble averages (theoretically expected charge and number of zeros). While for the minimum spacing $\delta = 2^{-10}$ there is no qualitative difference between the two algorithms, differences in performance become clear at lower data resolution. Twisted PhaseJumps performs well with a grid spacing of at least $\delta = 2^{-4}$, whereas Twisted PhaseJumps-coarse performs much more poorly with $\delta = 2^{-7}$. A more detailed post-hoc analysis showed that this is mainly due to Step 1, where Twisted PhaseJumps-coarse excludes too many zeros.

5.4. Experiment 2. We use Twisted PhaseJumps to calculate the zero set and charges of 500 realizations of the STFT of the signal $f^1(t) = e^{-t^2/2}$ embedded in complex white noise, with window $g(t) = te^{-t^2/2}$. The simulations are performed with a grid spacing parameter $\delta = 2^{-5}$ on the square $[-4, 4]^2$, but only zeros in $[-2, 2]^2$ are used, so as to minimize boundary effects. Fig. 6 compares the observed charge within an ever increasing counting box to ensemble averages provided by Proposition 3.10. In contrast to Experiment 1, due to the presence of a signal, the

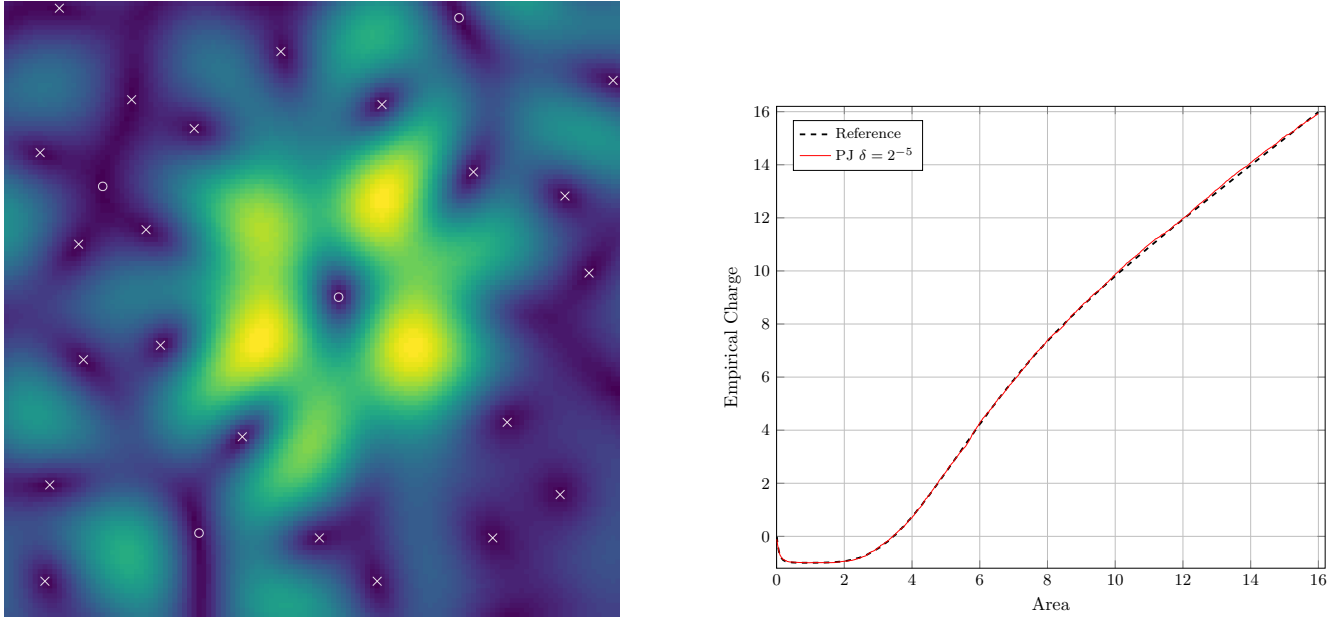


FIGURE 6. *Left*: One simulation of the STFT of a Gaussian signal in additive complex white noise using a first Hermite function as window (Modulus with positive charges marked by \times and negative charges marked by \circ). *Right*: Empirical charge based on 500 simulations on $[-2, 2]^2$ using the algorithms Twisted PhaseJumps (PJ) with $\delta = 2^{-5}$.

zero pattern is not stationary, and the particular choice of the counting boxes matters. We choose test boxes of increasing size in a spiral pattern from the center, so as to first capture the domain that is heavily affected by the deterministic signal component. We expect to see a quick drop of the empirical charge to -1 , corresponding to a negatively charged almost deterministic zero at the center, and then a smooth transition to the full charge on $[-2, 2]^2$, which is similar to the one obtained with no signal. The empirical curve follows the benchmark provided by Proposition 3.10 very closely.

5.5. Experiment 3. We illustrate the importance of the phase-stabilization factors in applications to the short-time Fourier transform. Fig. 7 shows the magnitude and phase of a single simulation of a STFT of complex white noise with window $g(t) = te^{-t^2/2}$. We note that phase varies very rapidly away from the origin, which could complicate computing winding numbers, and make the detection of zeros less reliable. To formalize and quantify this intuition, we compare the performance of the Euclidean stationary and the twisted version of PhaseJumps on STFT data (which use, respectively, Euclidean or twisted shifts in (1.4)). We simulate 5 realizations of the STFT of complex white noise with window $g(t) = te^{-t^2/2}$ on the square $[-32, 32]^2$ and with grid spacing $\delta = 2^{-5}$. As before, we only use the zeros in the smaller domain $[-16, 16]^2$, so as to minimize boundary effects. We count zeros and charges on boxes of increasing area following a spiral pattern from the center. We then expect the stationary and twisted versions of the algorithm to perform similarly for small test boxes (because these contain points near the origin where the twisted shifts do not play a significant role). As the testing area increases, we expect both algorithms to perform

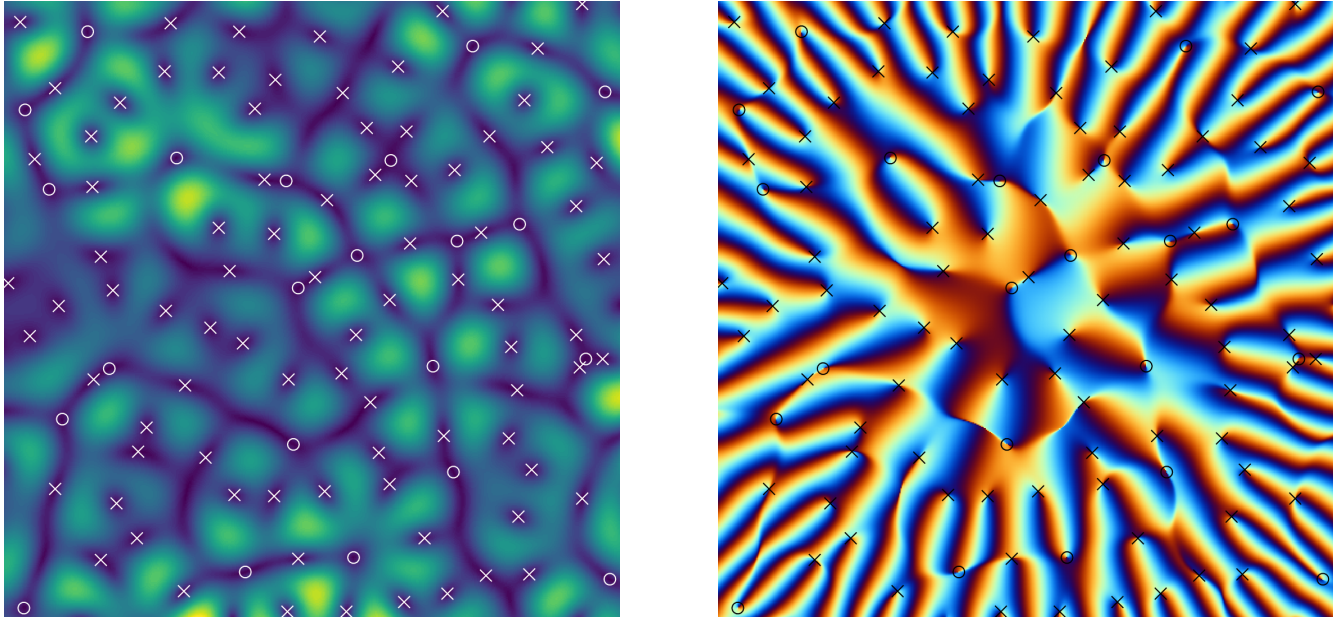


FIGURE 7. A simulation of the STFT of complex white noise using the first Hermite function as window (*Left*: Modulus with positive charges marked by \times and negative charges marked by \circ ; *Right*: Phase). While the modulus is stationary, the phase varies strongly away from the origin (here at the center).

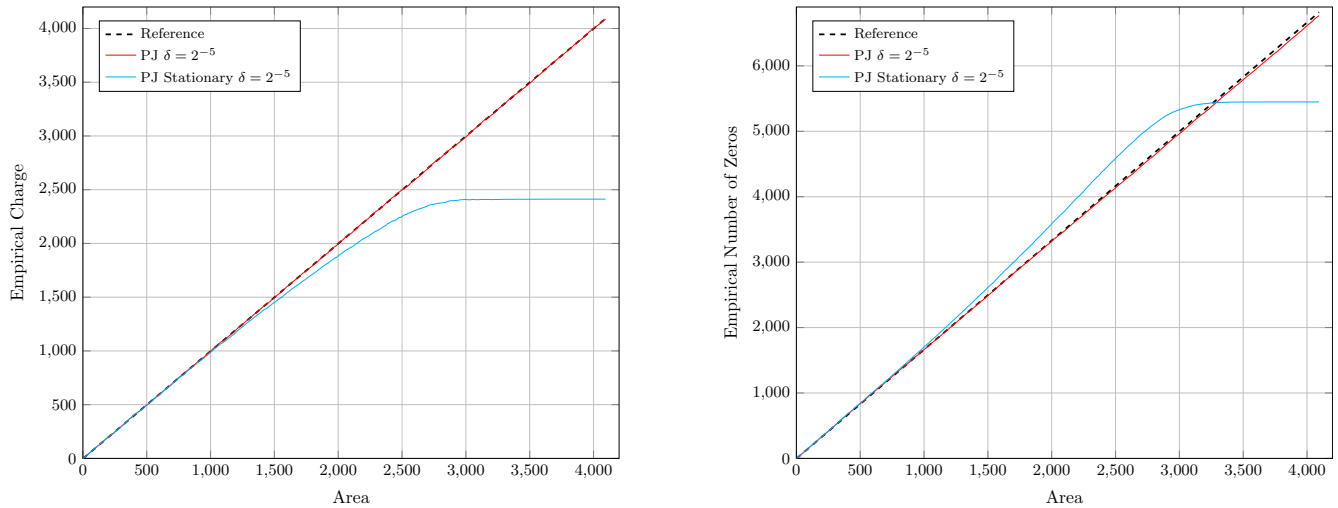


FIGURE 8. Empirical charge (left) and number of zeros (right) based on 5 simulations on $[-16, 16]^2$ using the algorithms Twisted PhaseJumps (PJ) and a Euclidean version (PJ Stationary) that does not use phase stabilization.

differently. The results, depicted in Fig. 8, confirm this. The computation ignoring the phase stabilization deviates from ensemble averages already for mid-range values of the testing area, while the twisted version tracks the benchmark closely.

REFERENCES

- [1] R. J. Adler and J. E. Taylor. *Random fields and geometry*. Springer Monographs in Mathematics. Springer, New York, 2007.
- [2] S. T. Ali, F. Bagarello, and G. Honnouvo. Modular structures on trace class operators and applications to Landau levels. *J. Phys. A*, 43(10):105202, 17, 2010.
- [3] G. Ascensi and J. Bruna. Model space results for the Gabor and wavelet transforms. *IEEE Trans. Inform. Theory*, 55(5):2250–2259, 2009.
- [4] J.-M. Azaïs and M. Wschebor. *Level sets and extrema of random processes and fields*. John Wiley & Sons, Inc., Hoboken, NJ, 2009.
- [5] J. Baber. Scaled correlations of critical points of random sections on Riemann surfaces. *J. Stat. Phys.*, 148(2):250–279, 2012.
- [6] R. Bardenet, J. Flamant, and P. Chainais. On the zeros of the spectrogram of white noise. *Appl. Comput. Harmon. Anal.*, 48(2):682–705, 2020.
- [7] R. Bardenet and A. Hardy. Time-frequency transforms of white noises and Gaussian analytic functions. *Appl. Comput. Harmon. Anal.*, 50:73–104, 2021.
- [8] Á. Bényi and K. A. Okoudjou. *Modulation Spaces: With Applications to Pseudodifferential Operators and Nonlinear Schrödinger Equations*. Applied and Numerical Harmonic Analysis. Birkhäuser Basel, 2020.
- [9] M. A. Colominas, G. Schlotthauer, and M. E. Torres. Improved complete ensemble emd: A suitable tool for biomedical signal processing. *Biomedical Signal Processing and Control*, 14:19–29, 2014.
- [10] M. A. Colominas, G. Schlotthauer, M. E. Torres, and P. Flandrin. Noise-assisted EMD methods in action. *Adv. Adapt. Data Anal.*, 4(4):1250025, 11, 2012.
- [11] J.-B. Courbot, A. Moukadem, B. Colicchio, and A. Dieterlen. Sparse off-the-grid computation of the zeros of stft. *IEEE Signal Process. Lett.*, 30:788–792, 2023.
- [12] M. R. Douglas, B. Shiffman, and S. Zelditch. Critical points and supersymmetric vacua. I. *Comm. Math. Phys.*, 252(1-3):325–358, 2004.
- [13] J. W. Eaton, D. Bateman, S. Hauberg, and R. Wehbring. *GNU Octave version 8.4.0 manual: a high-level interactive language for numerical computations*, 2023.
- [14] L. A. Escudero, N. Feldheim, G. Koliander, and J. L. Romero. Efficient Computation of the Zeros of the Bargmann Transform Under Additive White Noise. *Found. Comput. Math.*, 24(1):279–312, 2024.
- [15] N. Feldheim, A. Haimi, G. Koliander, and J. L. Romero. Hyperuniformity and non-hyperuniformity of zeros of gaussian Weyl-Heisenberg functions. *arXiv preprint: 2406.20003*.
- [16] P. Flandrin. Time–frequency filtering based on spectrogram zeros. *IEEE Signal Process. Lett.*, 22(11):2137–2141, 2015.
- [17] P. Flandrin. The sound of silence: Recovering signals from time-frequency zeros. In *2016 50th Asilomar Conference on Signals, Systems and Computers*, pages 544–548, 2016.
- [18] P. Flandrin. *Explorations in time-frequency analysis*. Cambridge University Press, 2018.
- [19] T. J. Gardner and M. O. Magnasco. Sparse time-frequency representations. *Proc. Nat. Acad. Sc.*, 103(16):6094–6099, 2006.
- [20] S. Ghosh, M. Lin, and D. Sun. Signal analysis via the stochastic geometry of spectrogram level sets. *IEEE Trans. Signal Process.*, 70:1104–1117, 2022.
- [21] A. Haimi and H. Hedenmalm. The polyanalytic Ginibre ensembles. *J. Stat. Phys.*, 153(1):10–47, 2013.
- [22] A. Haimi, G. Koliander, and J. L. Romero. Zeros of Gaussian Weyl-Heisenberg functions and hyperuniformity of charge. *J. Stat. Phys.*, 187(3):Paper No. 22, 41, 2022.
- [23] A. Haimi, L. Odellius, and J. L. Romero. Local repulsion between zeros and critical points of the Gaussian Entire Function. *ArXiv preprint: 2510.06821*, 2025.
- [24] J. H. Hannay. The chaotic analytic function. *J. Phys. A*, 31(49):L755–L761, 1998.
- [25] T. Hida. *Complex White Noise*, pages 232–251. Springer US, New York, NY, 1980.
- [26] J. B. Hough, M. Krishnapur, Y. Peres, and B. Virág. *Zeros of Gaussian analytic functions and determinantal point processes*, volume 51 of *University Lecture Series*. American Mathematical Society, Providence, RI, 2009.

- [27] J. W. Milnor. *Topology from the differentiable viewpoint*. Princeton Landmarks in Mathematics. Princeton University Press, Princeton, NJ, 1997. Based on notes by David W. Weaver, Revised reprint of the 1965 original.
- [28] F. Nazarov and M. Sodin. What is...a Gaussian entire function? *Notices Amer. Math. Soc.*, 57(3):375–377, 2010.
- [29] Z. Průša, P. L. Søndergaard, N. Holighaus, C. Wiesmeyr, and P. Balazs. The Large Time-Frequency Analysis Toolbox 2.0. In *Sound, Music, and Motion*, LNCS, pages 419–442. Springer International Publishing, 2014.
- [30] D. A. Spielman and S.-H. Teng. Smoothed analysis: an attempt to explain the behavior of algorithms in practice. *Commun. ACM*, 52(10):76–84, oct 2009.
- [31] M. Spivak. *Calculus on manifolds. A modern approach to classical theorems of advanced calculus*. W. A. Benjamin, Inc., New York-Amsterdam, 1965.
- [32] M. E. Torres, M. A. Colominas, G. Schlotthauer, and P. Flandrin. A complete ensemble empirical mode decomposition with adaptive noise. In *2011 IEEE international conference on acoustics, speech and signal processing (ICASSP)*, pages 4144–4147. IEEE, 2011.
- [33] N. L. Vasilevski. Poly-Fock spaces. In *Differential operators and related topics, Vol. I (Odessa, 1997)*, volume 117 of *Oper. Theory Adv. Appl.*, pages 371–386. Birkhäuser, Basel, 2000.
- [34] Z. Wu and N. E. Huang. Ensemble empirical mode decomposition: a noise-assisted data analysis method. *Adv. Adapt. Data Anal.*, 1(01):1–41, 2009.

(A. Haimi) FACULTY OF SCIENCE AND ENGINEERING, ÅBO AKADEMI UNIVERSITY, TUOMIOKIRKONTORI 3
20500 TURKU, FINLAND

Email address: antti.haimi@abo.fi

(G. Koliander) ACOUSTICS RESEARCH INSTITUTE, AUSTRIAN ACADEMY OF SCIENCES, DR. IGNAZ SEIPEL-
PLATZ 2, AT-1010 VIENNA, AUSTRIA

Email address: gkoliander@kfs.oeaw.ac.at

(J. L. Romero) FACULTY OF MATHEMATICS, UNIVERSITY OF VIENNA, OSKAR-MORGENSTERN-PLATZ 1, A-
1090 VIENNA, AUSTRIA, AND ACOUSTICS RESEARCH INSTITUTE, AUSTRIAN ACADEMY OF SCIENCES, DR. IGNAZ
SEIPEL-PLATZ 2, AT-1010 VIENNA, AUSTRIA

Email address: jose.luis.romero@univie.ac.at